

Absorption of Solar Radiation by O₂: Implications for O₃ and Lifetimes of N₂O, CFCl₃, and CF₂Cl₂

K. MINSCHWANER,¹ R. J. SALAWITCH, and M. B. MCELROY

Department of Earth and Planetary Sciences and Division of Applied Sciences, Harvard University, Cambridge, Massachusetts

An accurate line-by-line model is used to evaluate effects of absorption in the Schumann-Runge bands of O₂ on transmission of ultraviolet radiation. Allowing also for absorption in the Herzberg continuum, the model is shown to provide a reliable simulation of observed transmission in the spectral interval 192 to 200 nm. The model is used to evaluate rates for photolysis of N₂O, CFCl₃, and CF₂Cl₂, and to infer global loss rates (1.22×10^{10} kg N yr⁻¹, 7.21×10^7 and 3.04×10^7 kg Cl yr⁻¹, respectively) and instantaneous lifetimes (123, 44, and 116 years, respectively) appropriate for 1980. A parameterized version of the line-by-line model enabling rapid evaluation of transmission in the Schumann-Runge region is described. Photochemical calculations employing the parameterization and constrained by data from the Atmospheric Trace Molecule Spectroscopy experiment are used to examine the budget of odd oxygen. Consistent with previous studies, it is shown that photochemical loss of odd oxygen exceeds production by photolysis of O₂ for altitudes above 40 km. The imbalance between production and loss is shown to be consistent with a source of odd oxygen proportional to the product of the mixing ratio and photolysis rate of ozone, which suggests that processes involving vibrationally excited O₂ may play an important role in production of odd oxygen.

1. INTRODUCTION

Photodissociation of molecular oxygen in the optically allowed Schumann-Runge (S-R) bands and in the optically forbidden Herzberg continuum provides the dominant source of odd oxygen (O_x = O₃ + O) in the stratosphere and mesosphere. The Schumann-Runge bands represent the most important source of opacity for the spectral interval 175 to 200 nm, while the Herzberg continuum, extending from its threshold at 242 nm, makes a significant contribution to the opacity of the atmosphere at longer wavelengths.

Absorption in the S-R bands results in predissociation of the oxygen molecule; discrete absorption from the X³Σ_g⁻ ground state to the bound B³Σ_u⁻ state is followed by a nonradiative transition to either of the repulsive ¹Π_u, ³Π_u, ⁵Π_u, or ¹Σ_u⁺ states, resulting in production of two ground state atoms. Uncertainties relating to the complexity of spectral features in the S-R bands have persisted for the past two decades in treatments of the transmission of solar radiation in the 175- to 200-nm range [Kockarts, 1971; Hudson and Mahle, 1972; Park, 1974; Fang et al., 1974; Frederick and Hudson, 1980; Nicolet and Peetermans, 1980; Simon and Brasseur, 1983; World Meteorological Organization, 1986], with implications for production of O_x and for lifetimes of N₂O, CFCl₃, and CF₂Cl₂. The problem is associated with the paucity of laboratory data for S-R band absorption [Brix and Herzberg, 1954; Hudson and Carter, 1968; Ackerman et al., 1970]. The situation has improved more recently with values for S-R band spectral parameters based on laboratory studies by Yoshino et al. [1983, 1987] and Lewis et al. [1986a, b]. These data

were used by Murtagh [1988] and Nicolet and Kennes [1989] to obtain revised values of rates of photolysis in the S-R bands for the upper stratosphere and mesosphere.

The Herzberg continuum extends over the spectral interval 185 to 242 nm and is associated with the optically forbidden X³Σ_g⁻ → A³Σ_u⁺ transition in O₂. The unbound part of the A³Σ_u⁺ potential is accessed for wavelengths below 242 nm; absorption of solar radiation in the Herzberg continuum leads to dissociation of the O₂ molecule. There has been a downward trend in values of cross sections reported for the Herzberg continuum over the past 20 years. In situ measurements of solar irradiance in the stratosphere performed in the early 1980s [Frederick and Mentall, 1982; Herman and Mentall, 1982; Anderson and Hall, 1983] suggested that Herzberg cross sections in use at that time [e.g., Hasson and Nicholls, 1971; Shardanand and Prasad Rao, 1977] were too large by about 50%. The lower cross sections implied by the in situ data were confirmed subsequently by laboratory measurements [Johnston et al., 1984; Cheung et al., 1986b; Jenouvrier et al., 1986a, b]. The smaller cross sections obtained in the laboratory resulted from more careful analyses of the pressure dependence of absorption by O₂ in the Herzberg continuum [e.g., Cheung et al., 1986b]. Rates for photolysis of O₂ calculated using the new data for this spectral interval were presented by Nicolet and Kennes [1986].

Cross sections for absorption in the Herzberg continuum at shorter wavelengths, between 180 and 195 nm, were measured by Yoshino et al. [1992]; their data suggest that the cross section for the Herzberg continuum underlying the S-R bands is significantly less than expected on the basis of earlier data. Opacity contributed by the underlying Herzberg continuum affects the magnitude and height profile of the source for O_x and has, further, a critical influence on rates for photolysis of a variety of species, including N₂O, HNO₃, and the longer lived chlorofluorocarbon molecules [Froidevaux and Yung, 1982].

¹Now at National Center for Atmospheric Research, Boulder, Colorado.

Copyright 1993 by the American Geophysical Union.

Paper number 93JD00223.
0148-0227/93/93JD-00223\$05.00

Concentrations of O₃ calculated on the basis of photochemical models are sensitive to uncertainties in rates for photodissociation of O₂ [Froidevaux *et al.*, 1989], especially between 40 and 80 km where ozone is thought to be in photochemical steady state. The failure of current models to correctly reproduce measurements of O₃ from 40 to 80 km is well documented: calculated concentrations of ozone are lower than observed values by 30 to 60% at 50 km and the deficit grows to 40 to 80% at 80 km [Solomon *et al.*, 1983; Froidevaux *et al.*, 1985; Jackman *et al.*, 1986; Natarajan *et al.*, 1986; McElroy and Salawitch, 1989b]. The wide latitude assigned to cross sections for O₂ absorption (~40% uncertainty in the S-R bands and ~30% for the Herzberg continuum [DeMore *et al.*, 1990]) has led to suggestions that the discrepancy could be resolved, at least partly, by adjustments in O₂ cross sections [Solomon *et al.*, 1983; Clancy *et al.*, 1987; Froidevaux *et al.*, 1989; Allen and Delitsky, 1991]. Allen and Delitsky [1991] specifically targeted the uncertainty for photolysis in the S-R band and Herzberg continuum regions to account for the disagreement between calculated concentrations of ozone and values inferred from the ATMOS (Atmospheric Trace Molecule Spectroscopy) experiment. They found good agreement with observations when cross sections for absorption by O₂ were increased by 40% in both the S-R bands and Herzberg continuum. However, Clancy *et al.* [1987] concluded that adjustments in O₂ cross sections alone were insufficient to explain observations of ozone by the Solar Mesosphere Explorer.

Here we describe calculations for transmission of ultraviolet radiation based on a line-by-line representation of S-R band cross sections [Minschwaner *et al.*, 1992]. Calculated O₂ cross sections in the S-R bands and stratospheric transmittances in the 192- to 200-nm wavelength range are presented in section 2. Comparisons between the calculations and laboratory [Yoshino *et al.*, 1983] and in situ measurements [Anderson and Hall, 1986] establish that the S-R band description and values for Herzberg continuum cross section adopted here are appropriate for applications to the atmosphere. Rates for photolysis of N₂O, CFC₁₃, and CF₂Cl₂ are calculated in section 3, with resulting estimates for global loss rates and lifetimes for these gases. Photochemical calculations incorporating the new O₂ cross sections are discussed in section 4. Results are presented for the O_x budget of the stratosphere obtained from the Harvard photochemical model [Logan *et al.*, 1978], updated according to the S-R band parameterization described in the appendix and constrained by ATMOS measurements of radical and source gases [Farmer *et al.*, 1987]. The calculations do not support the hypothesis that the discrepancy in the O_x budget may be attributed to uncertainties associated with the absorption cross section of O₂ in the 175- to 242-nm wavelength range. The height profile for the missing source of O_x is, however, consistent with production of O_x due to photolysis at longer wavelengths of vibrationally excited O₂, as postulated by Slanger *et al.* [1988].

2. O₂ CROSS SECTIONS AND ATMOSPHERIC TRANSMISSION

Absorption of solar radiation in the spectral interval 175 to 200 nm is dominated by the S-R bands of O₂.

High-resolution laboratory data for absorption cross sections have been obtained for temperatures of 79 and 300 K [Yoshino *et al.*, 1983, 1987]. However, these cross sections are not directly applicable to studies of the stratosphere. We developed a full line-by-line representation of the S-R band system to allow computation of cross sections at stratospheric temperatures. Details of the line-by-line model are presented elsewhere [Minschwaner *et al.*, 1992]; only key features will be outlined here.

The line-by-line model employs the best available data for molecular constants, band oscillator strengths and predissociation line widths [Cheung *et al.*, 1986a, 1990; Yoshino *et al.*, 1983, 1987, 1990; Lewis *et al.*, 1986a, b]. It accounts for the triplet components of the principal R and P branches, allowing, in addition, for six satellite and two forbidden transitions. Principal branches of isotopically heavy oxygen are included [Cheung *et al.*, 1989; Yoshino *et al.*, 1989; Chiu *et al.*, 1990]. Rotational lines corresponding to $N'' = 1$ to 51 are considered for vibrational bands spanning the range 0-0 to 2-19. Populations of rotational and vibrational levels were evaluated assuming they can be represented by a Boltzmann distribution defined by the local temperature. Line shapes were calculated using Voigt profiles. Cross sections were determined by summing contributions from all absorption lines in a 500 cm⁻¹ window. Additional contributions to the absorption from the underlying S-R continuum were calculated by summing over Boltzmann-weighted partial cross sections [Allison *et al.*, 1971; Lewis *et al.*, 1985a, b].

Cross sections calculated in this manner are compared in Figure 1 with the measurements at 300 K by Yoshino *et al.* [1983]. The agreement is excellent and typical of that observed for the entire spectral range covered by the measurements (roughly 49,750 to 55,750 cm⁻¹, or 179 to 201 nm). Applications to the atmosphere require values for the absorption cross section over a range of tempera-

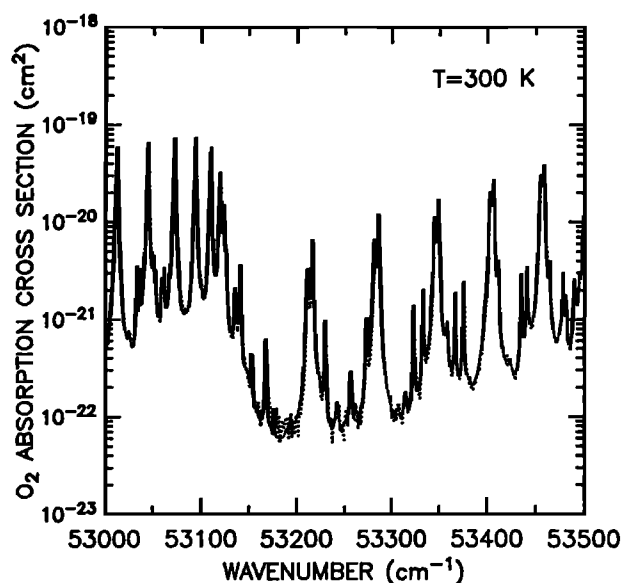


Fig. 1. Observed O₂ absorption cross section (dotted curve) [Yoshino *et al.*, 1983] and cross section calculated with the line-by-line model (solid curve) for a temperature of 300 K.

tures. We found in practice that significant computational savings could be realized by evaluating cross sections at a number of discrete temperatures, using these data to define a polynomial fit applicable for a range of atmospheric conditions. Cross sections obtained in this fashion were shown to accurately reproduce results of explicit line-by-line calculations at 0.5 cm⁻¹ resolution over the temperature range 130 to 500 K [Minschwaner *et al.*, 1992].

Figure 2 presents a comparison of calculated values of spectrally averaged transmission of solar radiation with measurements by Anderson and Hall [1986]. The data refer to the wavelength intervals 192.3–194.2, 194.2–196.1, 196.1–198.0, and 198.0–200.0 nm. The observational data were adjusted to account for absorption by O₃ and for Rayleigh scattering [Anderson and Hall, 1986]; thus the residual transmission indicated in Figure 2 should be due exclusively to effects of O₂. The model results were obtained assuming the temperature structure given by the U.S. Standard Atmosphere (1976). Values for the O₂ cross section in the Herzberg continuum were evaluated using the fit derived by A. Hall [Yoshino *et al.*, 1988] to the experimental data of Cheung *et al.* [1986b] and Jenouvrier *et al.* [1986a, b]. The good agreement between calculated and observed transmittances is consistent with simulations of transmission observed at high resolution, as reported earlier [Minschwaner *et al.*, 1992]. Calculations were also carried out using cross sections for the Herzberg continuum presented by Yoshino *et al.* [1992]. Agreement with the balloon observations was significantly poorer in this case; calculated transmittances were too large. We interpret the discrepancy to indicate that the choice of cross

sections for the Herzberg continuum by Yoshino *et al.* [1992], a function of the procedure used to describe absorption in the far wings of S-R lines, is inconsistent with the formulation adopted here for the S-R bands.

Figure 2 also includes values for transmittances determined according to data for the S-R bands and Herzberg continuum from the World Meteorological Organization (WMO) [1986] Assessment. The disagreement between the balloon measurements and transmittances from WMO [1986], noted previously by Anderson and Hall [1986], suggests that cross sections for either the S-R bands or Herzberg continuum, or both, must be too large in the WMO [1986] Assessment. To investigate this matter further, we performed a separate set of calculations involving absorption by the S-R bands alone. We found a persistent tendency for greater transmittance (lower S-R cross sections) in our calculations as compared to those based on the WMO data. The higher transmission calculated according to our S-R band cross sections, at least in three of the spectral intervals, is sufficient to account for between 30 and 40% of the disagreement shown in Figure 2. The remaining difference can be ascribed, most likely, to the lower values of cross sections employed for the Herzberg continuum in the present study (the value at 200 nm from Yoshino *et al.* [1988] is about 16% lower than the WMO [1986] recommendation).

The transmittances shown here agree closely with those calculated by Logan *et al.* [1978], using the formulation of Fang *et al.* [1974] updated with Herzberg continuum cross sections from Cheung *et al.* [1984]. This result is consistent with the findings of the intercomparison for O₂ and N₂O photolysis rates shown in Figures 12-8 and 12-9 of WMO [1986]. In that study, the Harvard model [Logan *et al.*, 1978] indicated deeper penetration of solar radiation in the S-R band region in comparison to other models [WMO, 1986].

The portion of the spectrum covered in Figure 2 includes the 2-0, 3-0, and 4-0 bands of the S-R system. In the absence of a high-resolution comparison, it is unclear whether the discrepancies in transmittance noted here result from differences in S-R cross sections for absorption lines or for the window regions between lines. Transmittances obtained by Murtagh [1988] were also larger than values recommended by WMO [1986]. He attributed the discrepancy in part to line widths in his calculation that were narrower than those employed by WMO [1986]. However, tables defining transmittance in the S-R bands presented by WMO [1986] are based on oscillator strengths and predissociation widths given by Frederick and Hudson [1979]; line widths recommended by these authors for the 2-0 band are 70% narrower than those employed here [Cheung *et al.*, 1990], while line widths for the 3-0 and 4-0 bands are only 3% and 8% larger (see Table II [Cheung *et al.*, 1990]). With the exception of the 2-0 band, there are no significant differences between the oscillator strengths presented by Frederick and Hudson [1979] and the values adopted for the present calculation (see Table 2 [Yoshino *et al.*, 1983]). It is possible that the discrepancy may reflect differences in the treatment of the hot bands (4-1, 5-1 and 6-1).

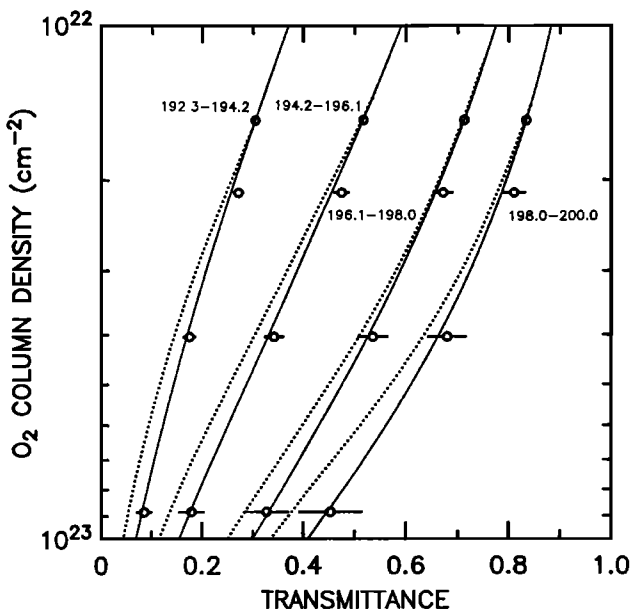


Fig. 2. Transmittance due to O₂ in the stratosphere measured by a balloon-borne spectrometer (circles) [Anderson and Hall, 1986] and calculated by the line-by-line model (solid curves), in four spectral intervals from 192.3 to 200.0 nm. The dotted curves denote transmittances obtained from WMO [1986], allowing for absorption by O₂ in both the S-R band and Herzberg continuum regions. The observations and WMO transmittances have been normalized to the line-by-line values at an O₂ column density of 1.53×10^{22} cm⁻².

3. LIFETIMES FOR N₂O, CFCl₃, AND CF₂Cl₂

The detailed treatment of the S-R bands described above allows for a quantitative assessment of rates for photolysis of atmospheric constituents that dissociate primarily in the 175- to 210-nm wavelength range. The spectral interval 190 to 210 nm, located at the tail of the S-R band absorption and at the head of the Hartley absorption band of O₃, is particularly important for photolysis of N₂O, CFCl₃ (CFC-11) and CF₂Cl₂ (CFC-12). Penetration of solar ultraviolet radiation for the spectral interval 175 to 240 nm is confined largely to a window centered at about 200 nm, as indicated in Figure 3. The influence of the S-R bands for wavelengths below 205 nm is evident in Figure 3, even with the moderately coarse resolution (1 nm) employed here. The importance of penetration in narrow spectral windows between individual S-R band absorption lines is more evident at higher resolution. Transmission calculated for a resolution of 0.002 nm is shown in Figure 4. Significant penetration is confined to spectral windows with widths typically as small as 0.2 nm. Transmission to lower altitudes is determined by: the cross section from absorption by O₂ in the wings of S-R absorption lines; the magnitude of the cross section for the underlying Herzberg continuum; and the contribution from the head of the Hartley band of O₃.

Cross sections for absorption of radiation by N₂O, CFCl₃, and CF₂Cl₂ vary slowly with wavelength compared with the extreme variability indicated for the S-R bands of O₂. As discussed in the appendix, photolysis frequencies can be evaluated to an accuracy of better than 10% using band transmittances. We choose, for present purposes, to use the line-by-line approach, accounting explicitly for the variation of temperature with altitude. We are able in this manner to minimize unnecessary numerical errors associated with evaluation of photolysis frequencies and lifetimes for the gases of interest here.

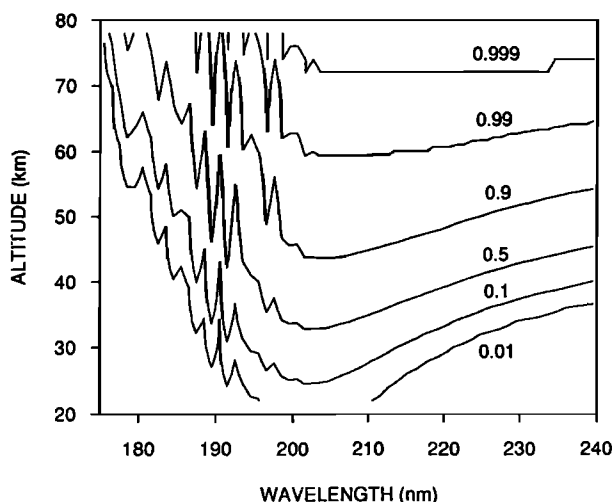


Fig. 3. Transmission of solar radiation calculated with the line-by-line model for the tropical atmosphere [Anderson *et al.*, 1986] and a solar zenith angle of 0°. Results have been averaged onto 1-nm spectral intervals for clarity of presentation. The S-R bands of O₂ represent the principal source of opacity for wavelengths less than 205 nm, while the Herzberg continuum of O₂ and the Hartley band of O₃ become important for longer wavelengths.

Cross sections for photodissociation of N₂O, CFCl₃, and CF₂Cl₂ were taken from DeMore *et al.* [1990]. Solar irradiances were specified according to measurements obtained by the Solar Ultraviolet Spectral Irradiance Monitor (SUSIM) [VanHoosier *et al.*, 1988], on board Spacelab 2 in 1985. Values for the solar irradiance in the SUSIM data set are quoted at 0.05-nm spectral intervals with a stated photometric error of 5% [VanHoosier *et al.*, 1988]. The SUSIM measurements indicate values for the solar irradiance that are about 15% larger than the WMO [1986] recommendations in the spectral region of the S-R bands, and about 3% higher in the Herzberg continuum [Nicolet and Kennes, 1988]. Altitude, latitude, and seasonal distributions of N₂O, CFCl₃, and CF₂Cl₂ were constructed using a combination of satellite and in situ data. Examples of profiles adopted for this purpose are illustrated in Figures 5, 6, and 7. Most of the measurements used to develop these climatologies were taken in the late 1970s and early 1980s. Concentrations of CFCl₃ and CF₂Cl₂ were scaled to represent conditions in 1980. Lifetimes and loss rates presented below are therefore appropriate for 1980.

Model profiles for N₂O were constrained to agree with balloon and aircraft measurements below about 35 km [Goldan *et al.*, 1980, 1981; Farmer *et al.*, 1980; Fabian *et al.*, 1981; Vedder *et al.*, 1981; Gallagher *et al.*, 1983; Gunson *et al.*, 1990], as indicated in Figures 5a and 5b. In the absence of in situ data, we used satellite observations from the Stratospheric and Mesospheric Sounder

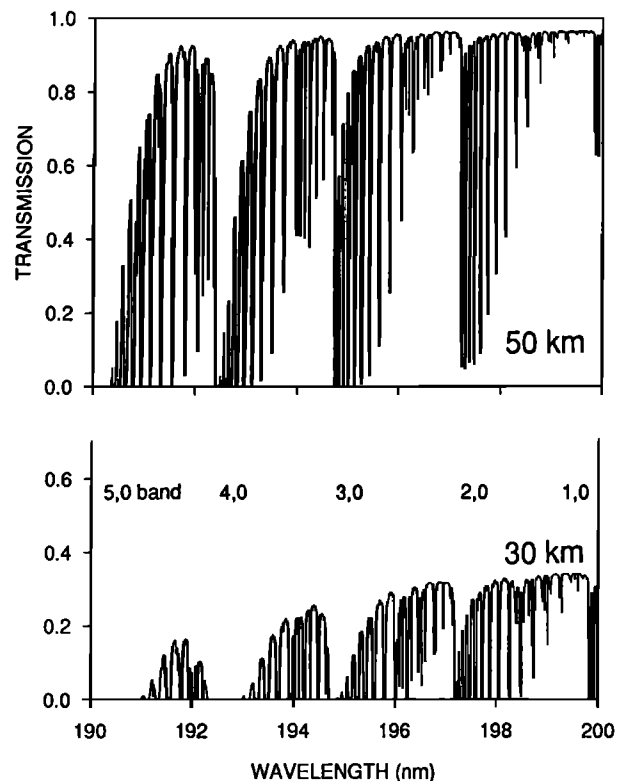


Fig. 4. Transmission of solar radiation calculated with the line-by-line model (0.002-nm resolution) at altitudes of 50 km (top panel) and 30 km (bottom panel), for the tropical atmosphere [Anderson *et al.*, 1986] and a solar zenith angle of 0°. Significant transmission of radiation to the middle and lower stratosphere occurs in narrow spectral regions between absorption lines in the S-R bands.

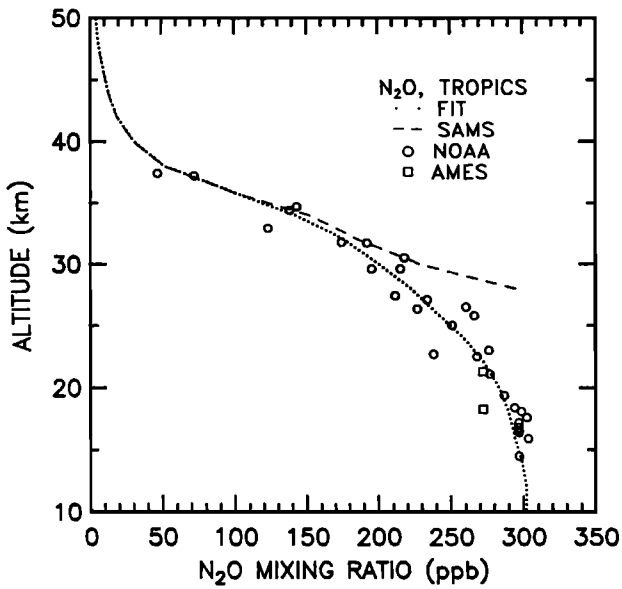


Fig. 5a. Vertical profiles of N₂O for the tropics, equinox. Circle denote balloon-borne measurements at 9°N and 5°S [Goldan et al. 1980, 1981]; squares represent aircraft measurements between 1.6°S and 9.9°N [Vedder et al., 1981]. The dashed curve refers to the average of SAMS satellite measurements at 5°N, equinox, between 1979 and 1981. The dotted curve indicates the vertical profile used here to estimate the lifetime of N₂O.

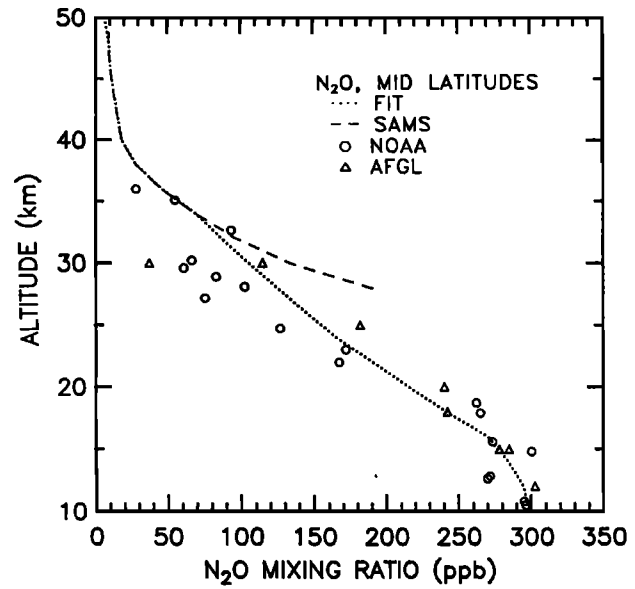


Fig. 5b. Vertical profiles of N₂O for mid-latitudes, equinox. Balloon-borne measurements at 41°N [Goldan et al., 1980, 1981] and 45°N [Gallagher et al., 1983] are denoted by circles and triangles, respectively. The dashed curve refers to the average of SAMS satellite measurements at 45°N, equinox, between 1979 and 1981. The dotted curve indicates the vertical profile used in this study for 45°N, equinox.

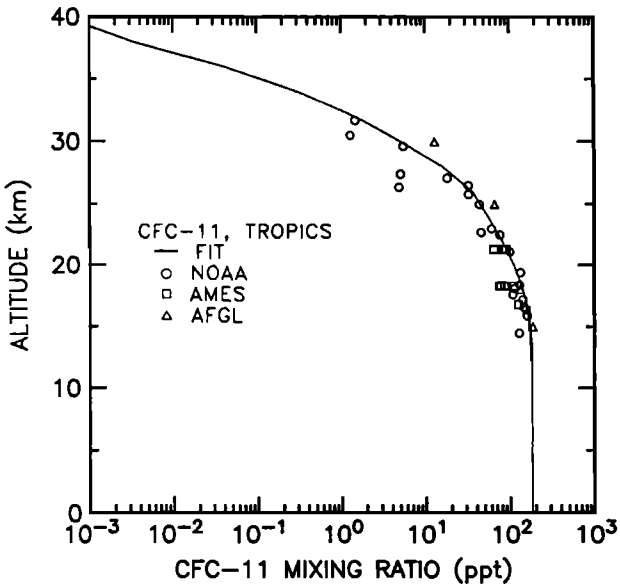


Fig. 6a. Vertical profiles for CFC₁₁, tropics. Balloon-borne measurements at 9°N and 5°S [Goldan et al., 1980, 1981] and 9°N [Gallagher et al., 1983] are denoted by circles and triangles, respectively; squares represent aircraft measurements between 1.6°S and 9.9°N [Vedder et al., 1981]. Observations have been scaled to values appropriate for 1980 by assuming a growth rate (independent of height) of 5.7% yr⁻¹. The solid curve refers to the vertical profile used in this study.

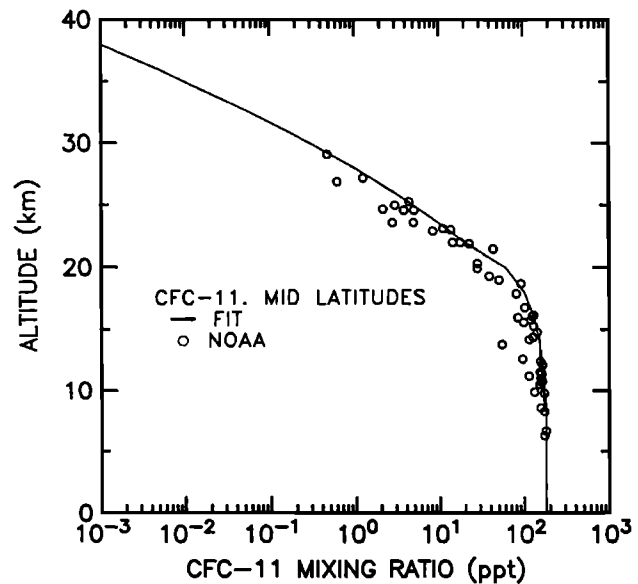


Fig. 6b. Vertical profiles for CFC₁₁, mid-latitudes. Same as Fig. 6a, except for a latitude of 45°N. Circles denote balloon-borne measurements at 41°N [Goldan et al., 1980, 1981].

(SAMS) instrument [Jones and Pyle, 1984] for altitudes above 35 km. It is relatively straightforward to constrain the model profiles to agree with both in situ and SAMS observations at low latitudes where the data sets are in reasonable agreement. Considerable difficulty was encountered at latitudes greater than about 30°N, where discrepancies between SAMS and in situ measurements are larger (Figure 5b). The approach used here

emphasized the balloon and aircraft data below altitudes of 25 to 30 km, with a smooth merge to SAMS observations above 35 km. As will be seen later, the global loss of N₂O occurs mainly at latitudes equatorward of 30°. Discrepancies between balloon and satellite data at higher latitudes are not expected to introduce significant error in our estimates for the global lifetime of N₂O.

Climatological distributions formulated for CFC₁₁ and CF₂Cl₂ were developed based on a combination of balloon and aircraft measurements by Heidt et al. [1975], Goldan et al. [1980], Fabian et al. [1981], Vedder et al.

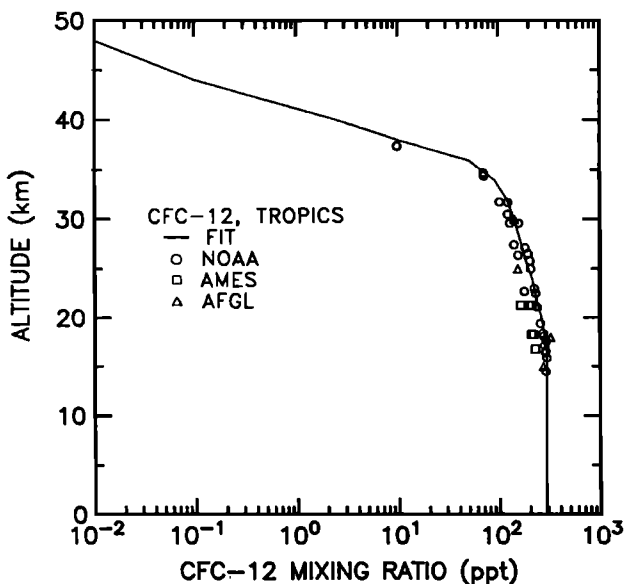


Fig. 7a. Vertical profiles for CF₂Cl₂, tropics. Same as Fig. 6a, except for CF₂Cl₂. The growth rate used to scale the balloon observations is 6.0% yr⁻¹.

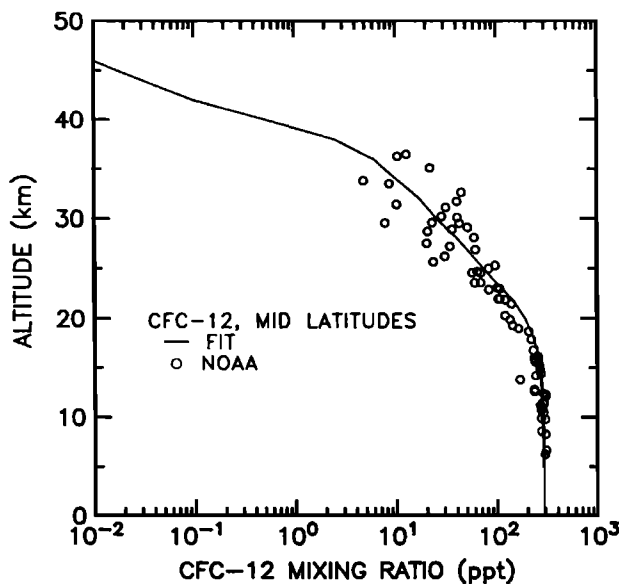


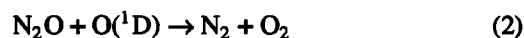
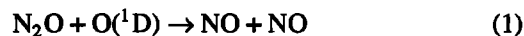
Fig. 7b. Vertical profiles for CF₂Cl₂, mid-latitudes. Same as Fig. 6b, except for CF₂Cl₂. The growth rate used to scale the balloon observations is 6.0% yr⁻¹.

[1981], and *Gallagher et al.* [1983]. The data were adjusted using temporal trends inferred from globally distributed surface measurements [*Cunnold et al.*, 1983a, b] to reflect concentrations expected for 1980. Mixing ratios for the 1980 troposphere were taken as 180 ppt for CFCl₃ and 290 ppt for CF₂Cl₂. The logarithm of the mixing ratios was assumed to decrease linearly with increasing altitude above 35 km, extrapolating trends implied by measurements at lower altitudes.

The variation of photolysis rates with wavelength for N₂O, CFCl₃, and CF₂Cl₂ is shown in Figures 8, 9, and 10, respectively. Photolysis rates for N₂O are largest at wavelengths between 195 and 205 nm over an altitude range of 25 to 35 km. There are significant contributions to the photolysis rate associated with windows in the S-R

band spectrum between 188 and 195 nm. Photolysis of CFCl₃ is important over approximately the same wavelength range as for N₂O, but the peak is shifted to lower altitudes by about 8 km. Photolysis of CF₂Cl₂ emphasizes shorter wavelengths than N₂O, but occurs in roughly the same altitude regime.

Photolysis represents the most important loss process for N₂O, CFCl₃, and CF₂Cl₂ [*World Meteorological Organization*, 1982]. Additional loss of N₂O arises as a consequence of reaction with O(¹D),



Reaction (1) provides, in addition, the dominant source of nitrogen radicals (NO_y = NO + NO₂ + NO₃ +

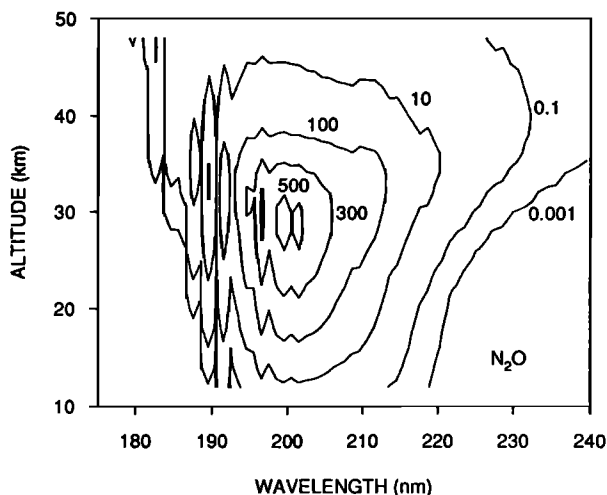


Fig. 8. Photolysis rate for N₂O (molecules cm⁻³ s⁻¹) calculated with the line-by-line model as a function of altitude and wavelength. Conditions correspond to equinox at 5° latitude, local noon. The N₂O profile shown in Fig. 5a has been used. Results have been integrated over 1-nm spectral intervals.

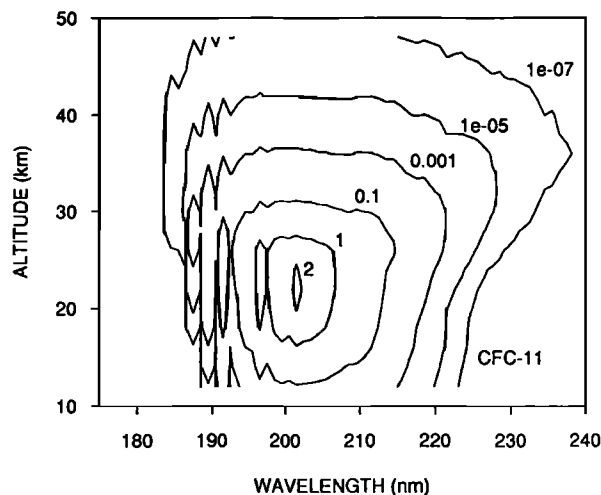


Fig. 9. Photolysis rate for CFCl₃ (molecules cm⁻³ s⁻¹) for the tropics, local noon. Same as Fig. 8, except the CFCl₃ profile shown in Fig. 6a has been used.

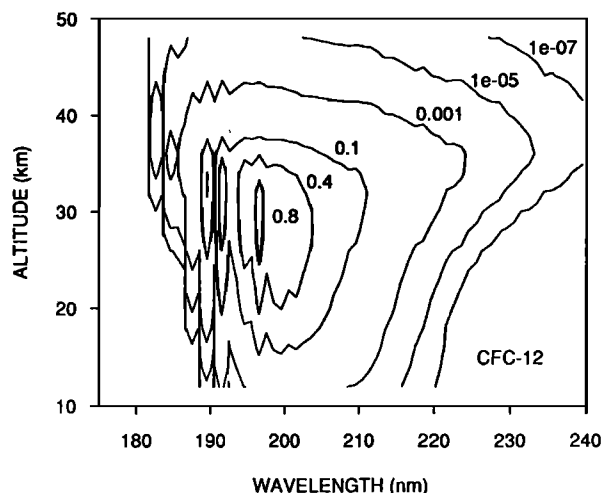


Fig. 10. Photolysis rate for CF₂Cl₂ (molecules cm⁻³ s⁻¹) for the tropics, local noon. Same as Fig. 8, except the CF₂Cl₂ profile shown in Fig. 7a has been used.

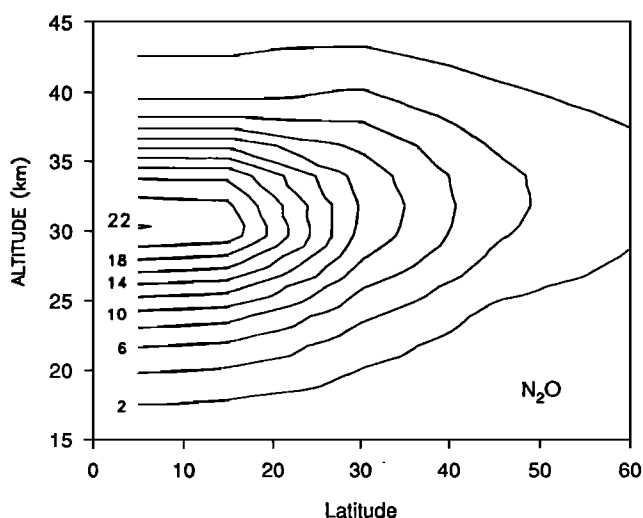


Fig. 11. Diurnally averaged loss rate for N₂O (10² molecules cm⁻³ s⁻¹) as a function of altitude and latitude, calculated with the line-by-line model, for equinox. The loss rate includes destruction of N₂O by reaction with O(¹D) as well as photolysis.

2 × N₂O₅ + HNO₂ + HNO₃ + HNO₄ + ClNO₃) in the stratosphere.

Loss rates for N₂O, CFCl₃, and CF₂Cl₂ were calculated for 1980 using the climatological distributions described above. We used the results from high-resolution calculations to determine diurnally averaged photodissociation frequencies for N₂O, CFCl₃, and CF₂Cl₂ as a function of latitude, altitude and season. The photodissociation frequency, or *J* value, for species “*i*” is given by

$$J_i(z) = \int_{\Delta\lambda} I(\lambda, z, \chi) \sigma_i(\lambda) d\lambda \quad (3)$$

where $I(\lambda, z, \chi)$ is the solar irradiance at wavelength λ , altitude z , and solar zenith angle χ ; $\sigma_i(\lambda)$ is the absorption cross section for species “*i*”; the integral is extended over the relevant wavelength range $\Delta\lambda$. The diurnally averaged *J* value was obtained by integrating equation

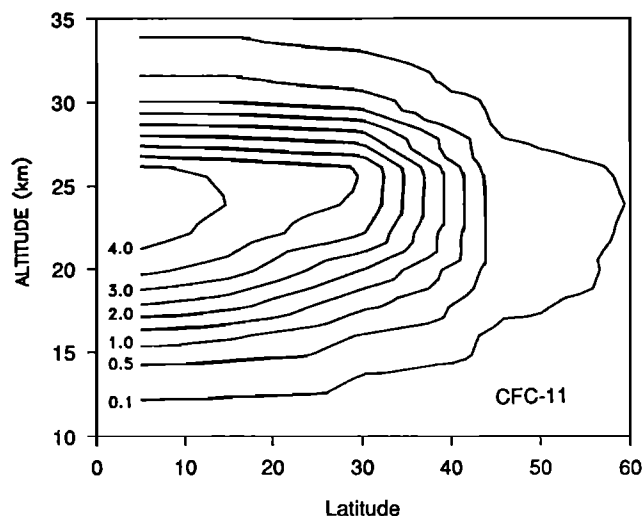


Fig. 12. Diurnally averaged loss rate for CFCl₃ (molecules cm⁻³ s⁻¹) as a function of altitude and latitude, calculated with the line-by-line model, for equinox. The loss rate was calculated assuming destruction of CFCl₃ by photolysis only.

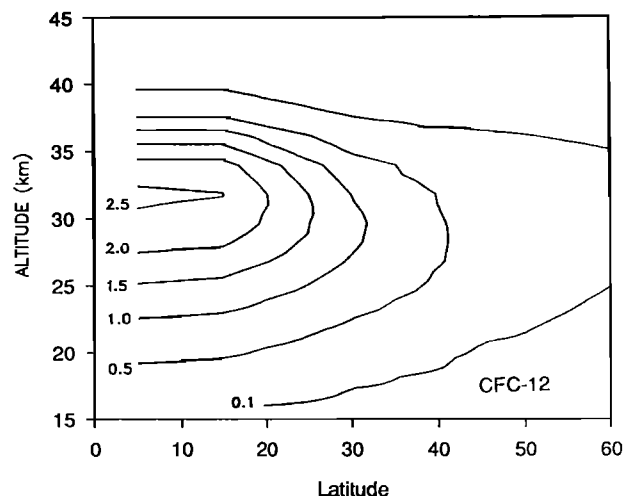


Fig. 13. Diurnally averaged loss rate for CF₂Cl₂ (molecules cm⁻³ s⁻¹). Same as Fig. 12 except for CF₂Cl₂.

(3) over a range of solar zenith angles appropriate for each latitude and season. Height, latitudinal, and seasonal profiles for pressure, temperature, and O₃ were taken from Anderson *et al.* [1986]. Concentrations of O(¹D) were evaluated using the Harvard photochemical model [Logan *et al.*, 1978], updated to account for recent information on reaction rates [DeMore *et al.*, 1990].

Meridional cross sections of the loss fields for N₂O, CFCl₃, and CF₂Cl₂ at equinox are displayed in Figures 11, 12, and 13. The general pattern of loss for N₂O depicted in Figure 11 is consistent with the studies by Johnston *et al.* [1979], Crutzen and Schmailzl [1983], and Ko *et al.* [1991]. As expected on the basis of the results presented in Figures 8–10, loss rates for N₂O and CF₂Cl₂ are largest in the 25- to 35-km altitude range (the contribution to the loss rate of N₂O due to reaction with O(¹D) accounts typically for about 10% of the total loss). The maximum in the loss rate for CFCl₃ occurs at somewhat lower altitudes, approximately 23 km. For all three constituents, the bulk of the removal is confined to the tro-

pics, reflecting larger values for rates of photolysis in this region and, for any given pressure level, higher mixing ratios resulting from upward transport from the troposphere.

The total loss rate, $L_i^{NH}(1980)$ for species "i" in the northern hemisphere in 1980 was obtained by integrating the local loss over latitude (with a resolution of 10° in the tropics, expanding to 15° at higher latitudes) and altitude (from the surface to 80 km), summing contributions for individual seasons (summer, equinox, and winter):

$$L_i^{NH}(1980) = \int dt \int dz \int n_i(\phi, z, t) F_i(\phi, z, t) \cos \phi d\phi \quad (4)$$

where $n_i(\phi, z, t)$ denotes the concentration (cm⁻³) of species "i" at latitude ϕ , altitude z , and time t , and $F_i(\phi, z, t)$ defines the corresponding value of the loss frequency (per second). For species removed solely by photolysis (CFCl₃ and CF₂Cl₂), F_i is given by the photolysis frequency defined above:

$$F_i(\phi, z, t) = J_i(\phi, z, t) \quad (5)$$

The loss frequency for N₂O includes a contribution due to reactions (1) and (2)

$$F_{N_2O}(\phi, z, t) = J_{N_2O}(\phi, z, t) + (k_1 + k_2) [O(^1D)] \quad (6)$$

where k_1 and k_2 denote rate constants for reactions (1) and (2) [DeMore *et al.*, 1990]. Global loss rates were calculated assuming equal contributions from the two hemispheres. Errors introduced by this assumption are expected to be small since, as noted above, most of the loss occurs in the lower stratosphere in the tropics where interhemispheric gradients of concentrations are relatively small. Loss rates for N₂O, CFCl₃, and CF₂Cl₂ are summarized in Table 1.

Global emissions for 1980, obtained by summing values for the annual loss and for the increase in inventory of individual gases, are listed also in Table 1. The increase in inventory for N₂O during 1980 was estimated based on the observed trend of about 0.2% yr⁻¹ [Weiss, 1981], and implies a source for N₂O of 1.52 × 10¹⁰ kg N yr⁻¹. The preindustrial abundance of N₂O was about 5% less than the 1980 value (285 ppb compared with 300 ppb) [Khalil and Rasmussen, 1988]. By scaling the removal rate for N₂O given in Table 1, we estimate a steady state source for the preindustrial atmosphere of about 1.16 × 10¹⁰ kg N yr⁻¹. Global production of N₂O appears to have risen by 31% over the past few hundred years. The increase is usually attributed to diverse forms

of agricultural activity [McElroy, 1976] but is not well understood.

Increases observed in inventories of CFCl₃ and CF₂Cl₂ in the atmosphere during 1980, 5.7% yr⁻¹ and 6.0% yr⁻¹ [Cunnold *et al.*, 1983a, b], provide the dominant contribution to the global emissions estimated in Table 1. The implied sources for CFCl₃ and CF₂Cl₂, 2.47 × 10⁸ and 2.41 × 10⁸ kg Cl yr⁻¹, are larger than values quoted by industry for 1980, 2.04 × 10⁸ kg Cl yr⁻¹ for CFCl₃ and 2.29 × 10⁸ kg Cl yr⁻¹ for CF₂Cl₂ [Chemical Manufacturers Association, 1982]. Global emissions estimated by the Chemical Manufacturers Association (CMA) for 1980 include approximate contributions from the former U.S.S.R. and Eastern Europe, amounting to 5% of the total for CFCl₃ and 15% for CF₂Cl₂. It seems unlikely that the uncertainty associated with this contribution for CFCl₃ could account for the disagreement with the value reported here; calculated emissions exceed the CMA estimate by 21%. This discrepancy is, however, consistent with recent simulations using a chemical tracer model (CTM) [Kao *et al.*, 1992]. When initialized with CMA estimates of global emissions for the period 1979 to 1982, the CTM indicated trends in CFCl₃ approximately 20% lower than observed over the same period.

The instantaneous lifetime of species "i" for 1980, $\tau_i(1980)$, may be defined as the ratio of its atmospheric inventory to the global removal rate:

$$\tau_i(1980) = \frac{\int dz \int n(\phi, z, 1980) \cos \phi d\phi}{2L_i^{NH}(1980)} \quad (7)$$

where the integral over latitude is extended to include both hemispheres. As indicated in Table 1, the instantaneous lifetimes for N₂O, CFCl₃, and CF₂Cl₂ are calculated to be 123, 44, and 116 years, respectively. The largest contribution to the uncertainty in lifetimes calculated here originates from the climatologies used to describe the distributions of these gases. We estimate uncertainties in the concentrations at latitudes and altitudes where the removal rate is maximum to be 15% for N₂O, and 20% for CFCl₃ and CF₂Cl₂. Accounting for uncertainties in the solar flux (5% [VanHoosier *et al.*, 1988]), the absorption cross section for O₂ (15% in the S-R bands [Minschwaner *et al.*, 1992], 10% in the Herzberg continuum [Nicolet and Kennes, 1988]), and the absorption cross section of each gas (20%, 10%, and 10% for N₂O, CFCl₃, and CF₂Cl₂, respectively [DeMore *et al.*, 1990]), we estimate associated uncertainties in loss rates and lifetimes to be 25 to 30%.

TABLE 1. Summary of Global Loss Rates and Atmospheric Lifetimes for N₂O, CFCl₃, and CF₂Cl₂

	Inventory (1980)	Annual Removal Rate (1980)	Instantaneous Lifetime, years	Annual Increase in Inventory	Implied Global Source
N ₂ O	1.50 × 10 ¹² kg N	1.22 × 10 ¹⁰ kg N yr ⁻¹	123	3.00 × 10 ⁹ kg N	1.52 × 10 ¹⁰ kg N yr ⁻¹
CFCl ₃	3.07 × 10 ⁹ kg Cl	7.21 × 10 ⁷ kg Cl yr ⁻¹	44	1.75 × 10 ⁸ kg Cl	2.47 × 10 ⁸ kg Cl yr ⁻¹
CF ₂ Cl ₂	3.51 × 10 ⁹ kg Cl	3.04 × 10 ⁷ kg Cl yr ⁻¹	116	2.11 × 10 ⁸ kg Cl	2.41 × 10 ⁸ kg Cl yr ⁻¹

For gases whose concentrations are changing significantly with time, values for instantaneous lifetimes differ from lifetimes in steady state due largely to temporal changes in abundances for the troposphere relative to the stratosphere. Net input to the atmosphere exceeds contemporary loss for N₂O, CFCl₃, and CF₂Cl₂. We expect in this case that the instantaneous lifetime should be somewhat longer than the lifetime in steady state; stratospheric abundances lag behind tropospheric levels reflecting the relatively sluggish rate at which air is exchanged between the troposphere and stratosphere [Schmidt and Khedim, 1991]. The distinction between instantaneous and steady state lifetimes is trivial for N₂O; increases of 0.2% yr⁻¹ in tropospheric concentrations have a negligible influence on the relative abundance between the stratosphere and troposphere for exchange times less than 5 years. It is significant, however, for CFCl₃ and CF₂Cl₂. Lifetimes in steady state, for which input to the atmosphere is assumed to balance loss, are estimated to be 41.5 years for CFCl₃ and 102 years for CF₂Cl₂.

The lifetime obtained here for N₂O, 123 years, is considerably shorter than the value of 175 years calculated by Johnston *et al.* [1979]. The difference is attributed most likely to discrepancies in cross sections used for the S-R bands and Herzberg continuum. Comparison of present results with lifetimes based on two-dimensional model studies [Ko and Sze, 1982; Jackman and Guthrie, 1985; Guthrie *et al.*, 1990; Ko *et al.*, 1991] is complicated by the details of the distributions of these gases calculated by the model, which depend in each case on the effects of transport and photochemical loss. Ko and Sze [1982] employed O₂ cross sections that were probably too large, resulting in *J* values smaller than those obtained here, leading therefore to larger values for steady state lifetimes (159, 65, and 135 years, for N₂O, CFCl₃, and CF₂Cl₂, respectively). The range of lifetimes given by Jackman and Guthrie [1985] indicate the sensitivity of two-dimensional model lifetimes to changes in O₂ cross sections; shortest lifetimes were obtained using cross sections for the Herzberg continuum similar to values used here.

A recent study by Ko *et al.* [1991] obtained lifetimes for N₂O of about 140 years using the SAMS distribution (assuming all the loss occurs in the region of the SAMS measurements), and 110 years using the distribution calculated by a 2-D model. Ko *et al.* [1991] appear to have used *J* values for N₂O that are similar to ours. We obtain lifetimes for N₂O similar to those given by Ko *et al.* [1991] using the SAMS distribution. Nevertheless, their 2-D model lifetime for N₂O is about 11% smaller than the lifetime reported here. The shorter N₂O lifetime obtained by Ko *et al.* [1991] is the result, most likely, of higher concentrations of N₂O calculated by their model above 35 km in the tropics as compared to the SAMS measurements used in our study. Steady state lifetimes for CFCl₃ and CF₂Cl₂ obtained here are in excellent agreement with values reported by Ko *et al.* [1991].

4. PRODUCTION AND LOSS OF ODD OXYGEN

Observations from the ATMOS experiment [Farmer *et al.*, 1987] provide a unique test of the reliability of models for the chemistry of the mid-latitude stratosphere.

Simultaneous measurements of profiles for O₃, NO, NO₂, N₂O₅, HNO₃, HNO₄, ClNO₃, HCl, H₂O and CH₄ were obtained from April 29 to May 6, 1985 for sunrise at 47°S, and for sunset at 30°N [Raper *et al.*, 1987; Russell *et al.*, 1988; Rinsland *et al.*, 1989; Gunson *et al.*, 1990; Zander *et al.*, 1990]. Earlier analyses comparing concentrations of O₃ observed by ATMOS with values calculated using constraints imposed by ATMOS measurements of radical and source gases concluded that loss of O_x exceeds production over most of the upper stratosphere in both hemispheres [McElroy and Salawitch, 1989b; Natarajan and Callis, 1989; Allen and Delitsky, 1991]. Our approach here is to use the treatment for O₂ photolysis described above to define the pattern of the missing source of odd oxygen implied by the ATMOS observations for altitudes between 30 and 60 km: abundances of O and O₃ are controlled mainly by photochemical processes in this region. The missing source of O_x is shown to be consistent with the pattern expected from photodissociation of vibrationally excited O₂ [Slanger *et al.*, 1988; Toumi *et al.*, 1991].

Data from ATMOS were used to specify vertical profiles for O₃, NO_y, Cl_y (HCl + ClNO₃ + ClO + HOCl + Cl₂ + Cl + 2 × Cl₂O₂), H₂O, CH₄, and temperature. Profiles for individual species within the NO_y, Cl_y, and HO_x (H + OH + HO₂ + 2 × H₂O₂) families of gases were obtained by solving the appropriate set of coupled time-dependent equations [Logan *et al.*, 1978; Prather *et al.*, 1984], using reaction rates and cross sections from DeMore *et al.* [1990]. Transmission of solar radiation and rates for photolysis of O₂ were calculated based on the procedure outlined in the appendix. Profiles for NO_y were constrained using ATMOS observations of NO, NO₂, ClNO₃, HNO₃, and N₂O₅ for altitudes below 53.5 km (where data for ClNO₃, HNO₃, or N₂O₅ are unavailable from ATMOS, model values for the concentrations of these gases were combined with ATMOS measurements to estimate NO_y; adjustments to NO_y from model values never exceeded 10%). The NO_y profile was assumed to be independent of height for altitudes above 53.5 km. Profiles for Cl_y were obtained by combining ATMOS measurements of HCl and ClNO₃ with model values for the concentrations of ClO and HOCl for altitudes below 55 km; at higher altitudes, the mixing ratio of Cl_y was assumed to be constant, equal to the value inferred for 55 km. The value of Cl_y calculated in this fashion was not allowed to exceed 2.8 ppb, the maximum value for 1985 based on measurements of halogenated source gases [WMO, 1986]. Species of the HO_x family were assumed to be in photochemical steady state, and concentrations were calculated using ATMOS measurements of H₂O and CH₄ combined with profiles of O(¹D) inferred from measurements of O₃. Since loss of O_x is dominated by processes involving hydrogen radicals at altitudes greater than 50 km, where ATMOS measurements of H₂O, CH₄, and O₃ are available to allow calculation of the key HO_x species, assumptions concerning NO_y and Cl_y for this region are not critical.

Model results and ATMOS observations for individual Cl_y species at 30°N and 47°S, respectively, are compared in Figures 14a and 14b. The ATMOS data shown for ClO at 30°N represent upper limits. Model results shown

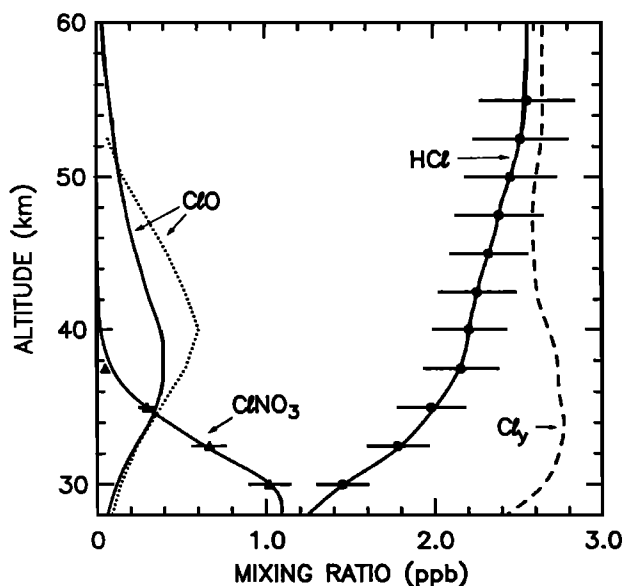
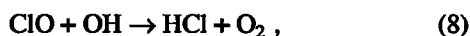


Fig. 14a. Calculated profiles for HCl, ClNO₃, and ClO (solid curves, as indicated) for the ATMOS simulation for 30°N, May 1, sunset, using Cl_γ (dashed curve) inferred from ATMOS measurements. Measurements of HCl and ClNO₃ and an upper limit for ClO obtained from ATMOS are indicated by the circles, triangles, and dotted curve, respectively; error bars represent 1 sigma estimate of the measurement uncertainty [Raper et al., 1987; Zander et al., 1990].

here assume a path for reaction of ClO with OH resulting in production of HCl,



with the branching ratio taken equal to 0.05, consistent with the upper limit (0.14) quoted by DeMore et al. [1990]. Calculations ignoring this path result in

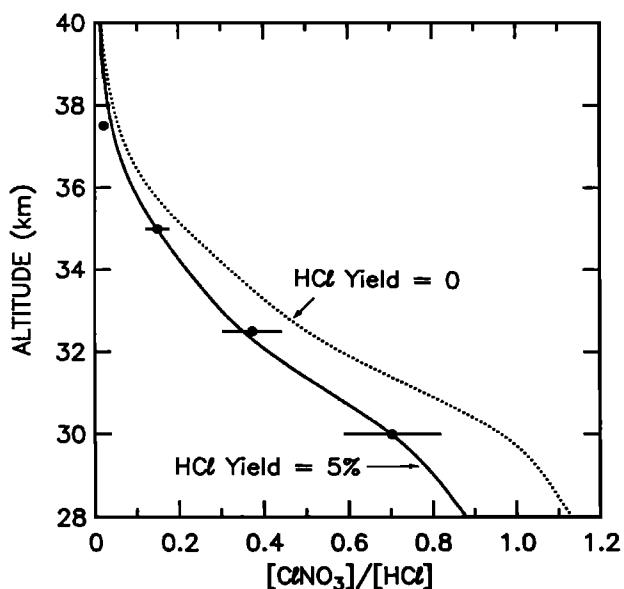


Fig. 15a. Calculated value of the ratio [ClNO₃]/[HCl], for the ATMOS simulation at 30°N, May 1, sunset, for a model using a branching ratio for HCl production by reaction (8) of 0.05 (solid curve) and 0.0 (dotted curve). The value of the ratio measured by ATMOS and the 1 sigma estimate of the uncertainty is shown by the circle with error bars [Zander et al., 1990].

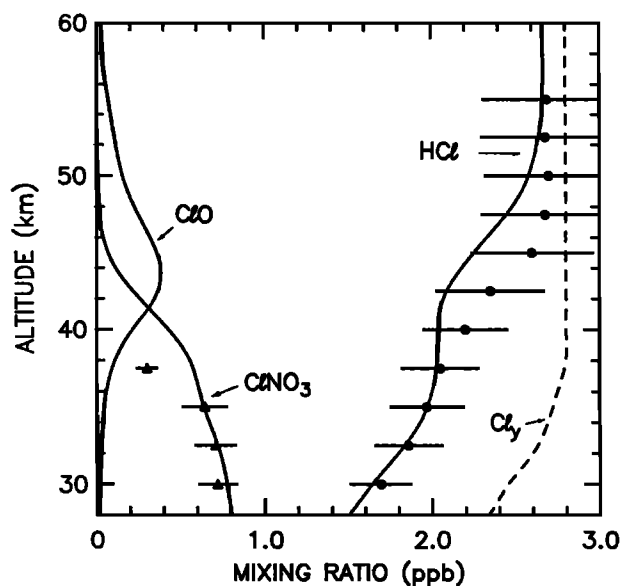


Fig. 14b. Same as Fig. 14a, except for 47°S, sunrise. An upper limit for ClO from ATMOS is not available for 47°S [Raper et al., 1987].

discrepancies for the ClNO₃ to HCl ratio larger than uncertainties permitted by the observations, as illustrated in Figure 15a and 15b, a point emphasized also by Natarajan and Callis [1991]. The possible importance of (8) was discussed also by McElroy and Salawitch [1989a] who argued that the inclusion of this process would result in improved agreement between calculated and observed profiles for ClO [Weinstock et al., 1981; Brune et al., 1988]. When the HCl path in (8) is included, values of ClO at 40 km are reduced by 20% and 30% for the simulations at 30°N and 47°S, respectively.

Simultaneous measurements of ClO and HCl obtained from thermal emission spectroscopy are consistent with models that allow for the HCl branch in reaction (8) [Stachnik et al., 1992]. Comparison of the observed annual

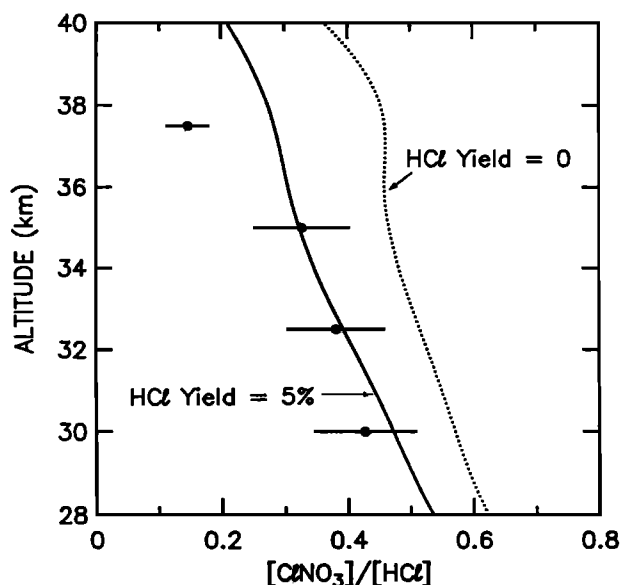


Fig. 15b. Same as Fig. 15a, except for 47°S, sunrise.

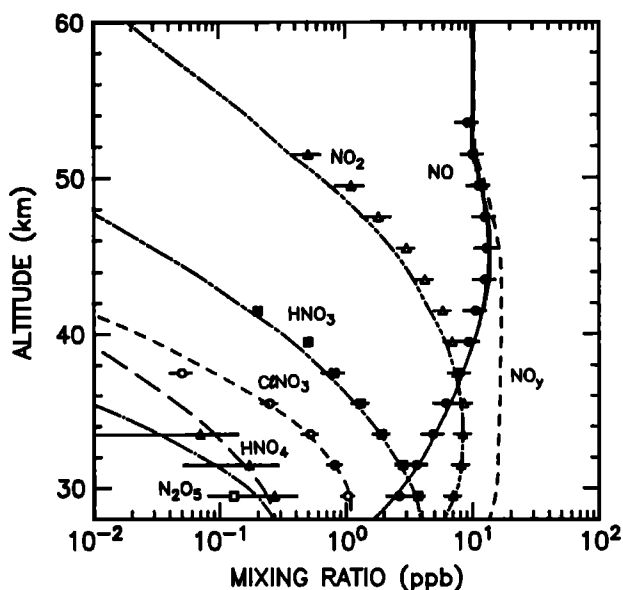


Fig. 16a. Calculated profiles for NO, NO₂, HNO₃, ClONO₂, N₂O₅, and HNO₄ (indicated curves) for the ATMOS simulation for 30°N, May 1, sunset, using NO_y inferred from ATMOS observations. Measurements obtained by ATMOS, and 1 sigma estimates of the error bars, are indicated for NO (solid circles), NO₂ (open triangles), HNO₃ (solid squares), ClONO₂ (open circles), HNO₄ (solid triangles), and N₂O₅ (open squares) [Russell et al., 1988; Zander et al., 1990].

amplitude of ozone to values calculated with a two-dimensional model provides further support for the HCl branch [Chandra et al., 1993]. Calculated reductions of ozone at 40 km due to the build up of anthropogenic fluorocarbons are 30% less for models that allow for the HCl path, with branching ratio equal to 0.14–0.15, compared to models that do not allow for HCl production by (8) [Brasseur et al., 1985; Chandra et al., 1993]. These findings underscore the need for further atmospheric and laboratory studies to define the kinetics of the processes that control the partitioning of gases within the Cl_y family.

Figures 16a and 16b present a comparison of results from the model with ATMOS observations for NO_y species at 30°N and 47°S, respectively. Agreement between observed and calculated profiles is excellent for both simulations. The profile for ClONO₂ is reproduced more accurately when we allow for production of HCl in (8), particularly near 36 km for the simulation at 47°S. The model result for the ratio of NO to NO₂ is larger than the measured value by about 30% for the higher altitudes at 30°N, but is nearly equal to the measured value at 47°S. Similar conclusions were reached by Allen and Delitsky [1990]. The measurement uncertainty for NO and NO₂ is approximately 30%. It is unclear whether the discrepancy at 30°N indicates a deficiency in the partitioning of NO and NO₂, which could reflect in particular an overestimate of the concentration of O, with potentially important implications for the budget of odd oxygen. For altitudes below 30 km, hydrolysis of N₂O₅ on the background sulfate aerosol alters the partitioning of the NO_y species [Cadle et al., 1975] and must be included in order to account for ATMOS observations of NO₂ and HNO₃, especially for the southern hemisphere [Natarajan and Callis, 1991; McElroy et al., 1992].

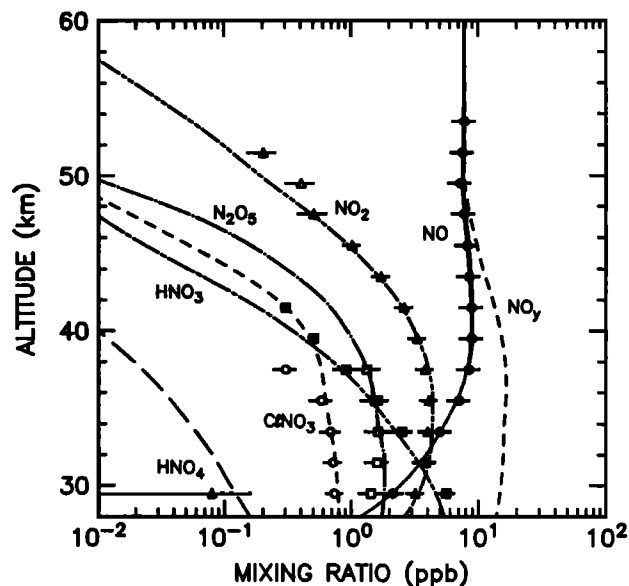
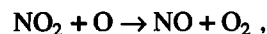


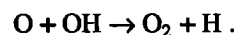
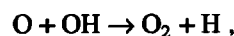
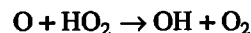
Fig. 16b. Same as Fig. 16a, except for 47°S, sunrise.

Model concentrations for OH are in reasonable agreement with balloon-borne measurements at mid-latitudes [McElroy and Salawitch, 1989a]. Model results for HO₂ and HOCl are compared with measurements obtained at 32°N during May 1988 [Chance et al., 1989; Traub et al., 1990] in Figures 17 and 18, lending further support to the validity of the model. Concentrations of OH and HO₂ are unaffected by production of HCl by reaction (8), while values of HOCl are reduced by approximately 20% at 40 km altitude when this path is included.

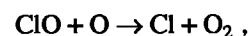
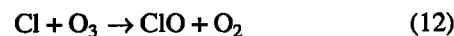
Rates calculated for the production and removal of O_x, illustrating the relative importance of the dominant catalytic loss processes, are presented in Figures 19a and 19b for the simulations at 30°N and 47°S, respectively. Loss of O_x is dominated at low altitudes by the catalytic sequence involving oxides of nitrogen,



and at high altitudes by sequences involving HO_x radicals,



The catalytic sequence involving chlorine radicals,



has its largest influence on the O_x budget near an altitude of 40 km; the direct recombination of O and O₃ contributes about 10% of the total loss of O_x at all altitudes.

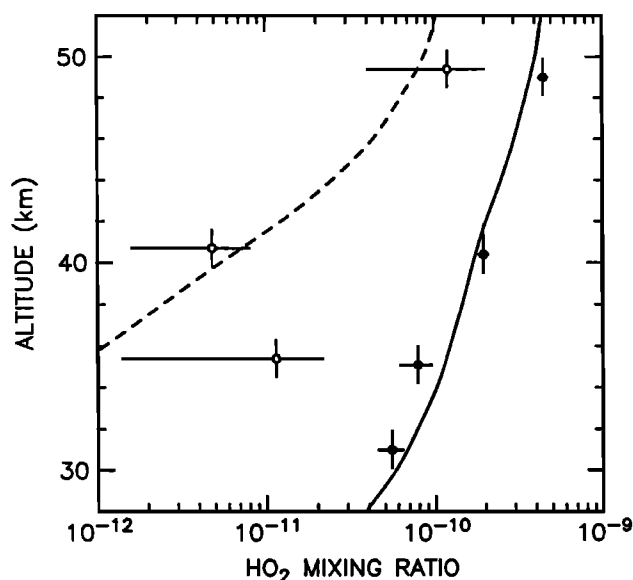


Fig. 17. Calculated profiles for HO₂ at 1500 UT (solid curve) and midnight (dashed curve) for the ATMOS simulation for 30°N, and data from Traub *et al.* [1990], obtained on May 12, 1988, at 32°N, at 1700 UT (solid circles) and 0100 UT (open circles). Horizontal error bars represent 2 sigma uncertainty of the measurement; vertical error bars indicate estimates of the uncertainty of the sampling altitude.

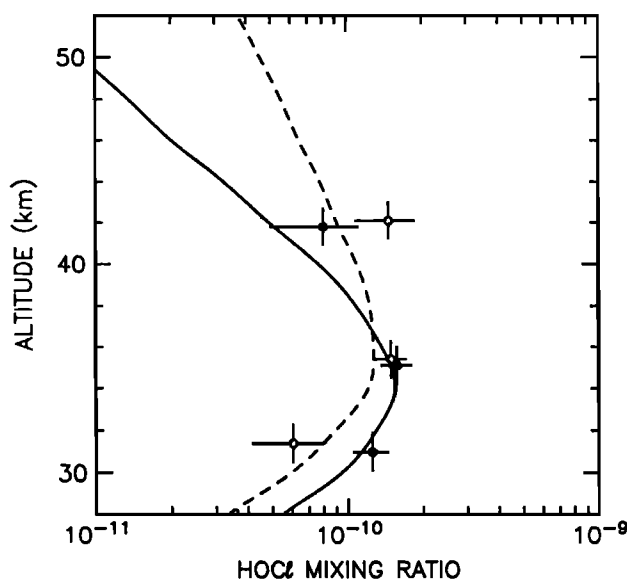


Fig. 18. Calculated profiles for HOCl at 1700 UT (solid curve) and midnight (dashed curve) for the ATMOS simulation for 30°N, and data from Chance *et al.* [1989], obtained on May 12, 1988, at 32°N, at 1700 UT (solid circles) and 0100 UT (open circles). Horizontal error bars represent 2 sigma uncertainty of the measurement; vertical error bars indicate estimates of the uncertainty of the sampling altitude.

Photolysis of O₂ provides the only source of O_x included in these simulations.

The difference between the rates calculated for loss and production of O_x is shown in Figures 20a and 20b for the simulations at 30°N and 47°S. Production and loss of O_x are nearly equal at an altitude of 40 km for both simulations. Loss of O_x exceeds production at higher altitudes, where removal of O_x is dominated by processes involving HO_x radicals. The imbalance of production and loss is larger and more sharply peaked near 50 km for the simulation at 30°N (summer) than for 47°S (winter). The challenge is to account for the pattern of the imbalance in terms either of a missing source of O_x or a reduction in the rate of the removal processes. The behavior found here is similar to that reported by McElroy and Salawitch [1989b], Natarajan and Callis [1989], and Allen and Delitsky [1991], except for the influence of the HCl path in reaction (8), which is responsible for a reduction of 13% in the loss rate of O_x calculated for 47°S at 40 km.

Allen and Delitsky [1991] suggested better agreement between production and loss of O_x could be achieved if absorption cross sections in the Herzberg and S-R regions were increased by 40%. We estimate that the uncertainty in the photolysis rate of O₂ calculated here should not exceed 20%, attributable to uncertainties in the absorption cross sections of 10% for the Herzberg region [Nicolet and Kennes, 1988] and 15% for the S-R region [Minschwaner *et al.*, 1992], photometric errors of 5% in solar irradiances [VanHoosier *et al.*, 1988], and maximum errors of 10% associated with the S-R band parameterization (see appendix). Cross sections for O₂ inferred by Anderson and Hall [1986] from measurements of the transmission of solar radiation in the stratosphere verify the recent laboratory measurements of the O₂ cross sections in the Herzberg continuum [Yoshino *et*

al., 1988], as discussed above, and would appear to exclude the adjustments suggested by Allen and Delitsky [1991]. Furthermore, a 40% increase in the absorption cross section of O₂ in both the Herzberg and S-R regions would lead to comparable increases in the production of O_x at all altitudes between 40 and 60 km, a pattern inconsistent with that shown in Figure 20a.

Slanger *et al.* [1988] suggested that photolysis of vibrationally excited O₂ in the ground electronic state X³Σ_g⁻ could provide a significant source of O_x. They allowed for formation of vibrationally excited O₂ by photolysis of O₃ through the B(1¹B₂) state, which predissociates leading to production of O₂(X³Σ_g⁻) and O(³P). They concluded that significant population of vibrational levels with v'' greater than 15 would be required for this mechanism to provide a significant source of O_x.

Toumi *et al.* [1991] estimated that this mechanism could enhance production of O_x by up to 60% at altitudes near 60 km. They calculated the concentration of vibrationally excited oxygen, O₂[‡], in vibrational level v'' by assuming steady state between production by photolysis of ozone (for wavelengths less than 300 nm) and quenching from the level above, and loss by vibration-to-vibration exchange with O₂(v''=0) and photolysis. With these assumptions, the concentration of O₂[‡] is given by

$$[\text{O}_2^{\ddagger}]_{v''} = \frac{0.13 \phi_{v''} J_{\text{O}_3} [\text{O}_3] + k_{v''+1} [\text{O}_2] [\text{O}_2^{\ddagger}]_{v''+1}}{k_{v''} [\text{O}_2] + J_{v''}} \quad (13)$$

where 0.13 represents the quantum yield for production of O₂(X³Σ_g⁻) due to photolysis of O₃ in the Hartley region, φ_{v''} is the quantum yield for production of level v'', J_{O₃} is the photodissociation frequency for O₃ at

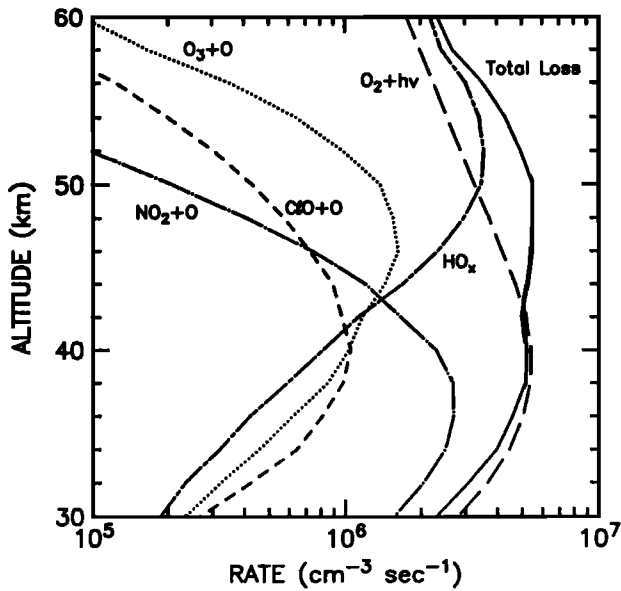


Fig. 19a. Diurnally averaged rates for production and loss of odd oxygen for the ATMOS simulation for 30°N, May 1, calculated with a photochemical model constrained by measured profiles for O₃, H₂O, and CH₄ [Gunson *et al.*, 1990] and inferred profiles for Cl_y and NO_y (Figs 14a and 16a). Photolysis of O₂ (long-dashed curve) is the only source of odd oxygen considered here. The total removal rate of O_x is given by the solid curve; removal rates for specific catalytic cycles are also given, as indicated (see text).

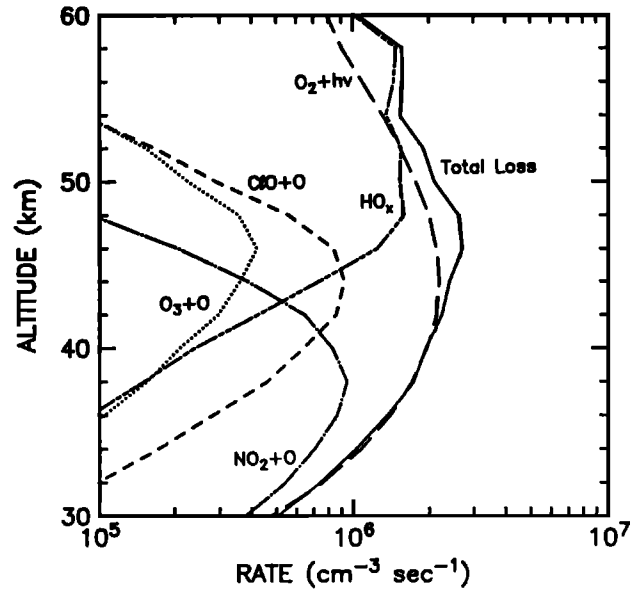


Fig. 19b. Same as Fig. 19a, except for the ATMOS simulation for 47°S (Cl_y and NO_y profiles from Figs 14b and 16b are used).

wavelengths less than 300 nm, $k_{v''}$ and $k_{v''+1}$ are the rate constants for quenching of levels v'' and $v''+1$, respectively, and $J_{v''}$ is the photodissociation frequency for level v'' . Taking $\phi_{v''}$ approximately constant with respect to altitude (as assumed by *Toumi et al.* [1991]) and noting that photolysis makes a minor contribution to the denominator of (13), the rate for production of O_x due to photolysis of O₂[‡] is given by

$$\begin{aligned} \text{Production of } O_x &= \sum_{i=1}^N J_i [O_2^{\ddagger}]_i & (14) \\ &\approx \frac{0.13 J_{O_3} [O_3]}{[O_2]} \sum_{i=1}^N \frac{J_i}{k_i} \sum_{j=i}^N \phi_j \\ &\approx C J_{O_3} f_{O_3} \end{aligned}$$

where f_{O_3} denotes the mixing ratio of O₃. We estimate a value for C of $1.9 \times 10^{14} \text{ cm}^{-3}$ based on results presented by *Toumi et al.* [1991].

The variation with altitude of J_{O_3} (24-hour average), the mixing ratio of O₃, and their product is shown in Figures 21a and 21b for the simulations at 30°N and 47°S, respectively. The value of $J_{O_3} \cdot f_{O_3}$ decreases at higher

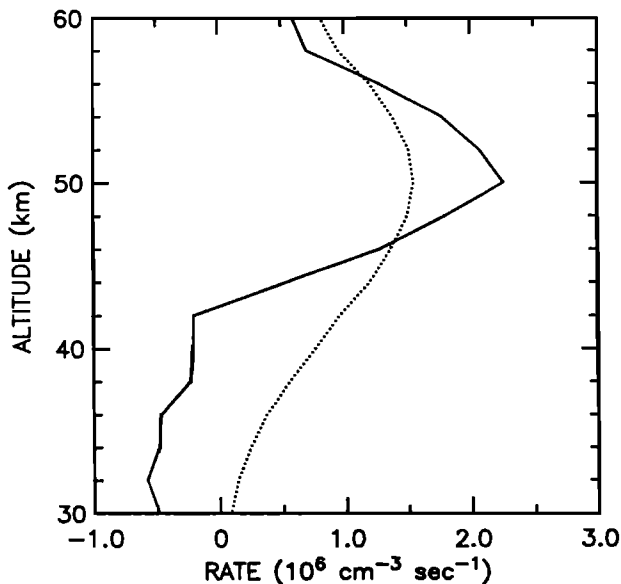


Fig. 20a. The imbalance between the diurnally averaged loss and production rates of odd oxygen (solid curve) for the ATMOS simulation for 30°N, May 1, and the source of odd oxygen from photolysis of O₂[‡] (dotted curve) inferred from the model results of *Toumi et al.* [1991].

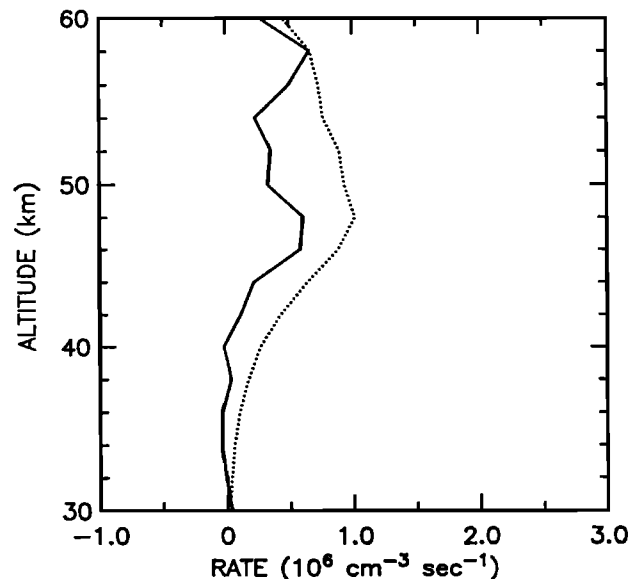


Fig. 20b. Same as Fig. 20a, except for the ATMOS simulation for 47°S.

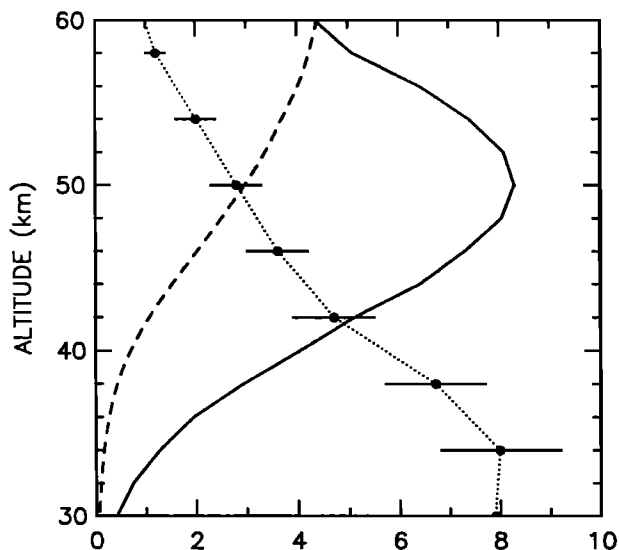


Fig. 21a. The mixing ratio of O₃ and the 1 sigma estimate of the uncertainty measured by ATMOS at 30°N (circle with error bars) [Gunson *et al.*, 1990], the diurnally averaged photolysis frequency of O₃ for wavelengths less than 300 nm for 30°N, May 1 (dashed curve), and the product of the ozone mixing ratio and the photolysis frequency (solid curve).

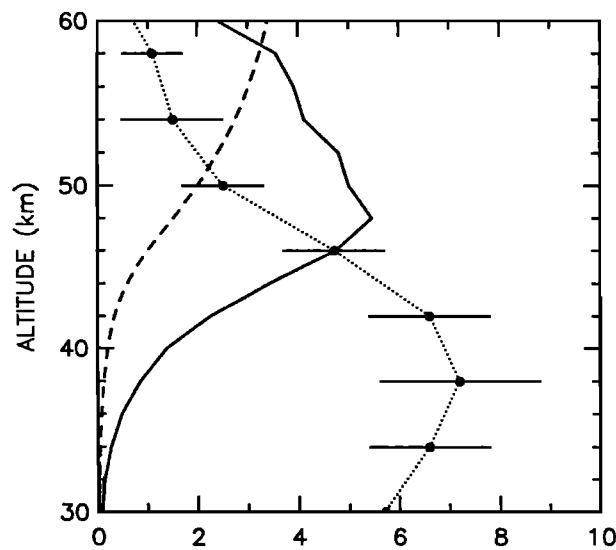
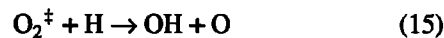


Fig. 21b. Same as Fig. 21a, except for 47°S.

altitudes due to the drop in the mixing ratio of O₃, and at lower altitudes because of the decline in the photolysis rate of O₃. The maximum value of $J_{O_3} \cdot f_{O_3}$ occurs at 50 km, the same altitude at which the imbalance between production and loss of O_x is greatest at 30°N. The value of $J_{O_3} \cdot f_{O_3}$ is less for 47°S (winter) than for 30°N (summer), consistent with lower values of the missing source of O_x for this region. The source of O_x from photolysis of O₂[‡] [equation (14)] is shown by the dotted curve in Figures 20a and 20b. We consider it particularly interesting that a source of O_x proportional to $J_{O_3} \cdot f_{O_3}$ can account for the general trends observed for the quite different insolation conditions in the two hemispheres.

The population of vibrationally excited states depends critically on the vibrational distribution of O₂ from photodissociation of ozone and on rates for collisional relaxation. Toumi *et al.* [1991] used values for $\phi_{v''}$ derived from a study of the photodissociation of O₃ at 226 nm [Kinugawa *et al.*, 1990] for all wavelengths less than 300 nm. However, higher vibrational levels ($v'' > 15$) are less likely to be produced by photolysis of O₃ at longer wavelengths. Toumi [1992] presented a more detailed account of O₂[‡] photochemistry including an approximate treatment for the wavelength dependence of $\phi_{v''}$ and allowing for two quanta vibrational transfer in the quenching of O₂[‡]. Production of O_x was found to be significantly smaller than postulated earlier by Toumi *et al.* [1991], due primarily to the reduction in the generation of higher vibrational levels of O₂[‡] [Toumi, 1992]. There remain significant uncertainties in several key processes, however, especially the wavelength dependence of $\phi_{v''}$ and rates for collisional relaxation. These uncertainties underscore the need for further laboratory studies to better define the photochemistry of O₂[‡].

Our results would not exclude additional potential sources of O_x that also depend on O₂[‡]. For example, a source due to reaction of O₂[‡] with H,



could also play a role, since this reaction is exothermic for $v'' \geq 4$. Reaction (15) could also provide a significant source of OH. Additional production of OH appears to be required in order to account for the column measurements of Burnett *et al.* [1988]. A careful analysis based on experimental data for rates of reaction involving O₂[‡] is required to complete our understanding of the possible role of excited states of O₂ on the chemistry of odd oxygen.

5. CONCLUDING REMARKS

The quantitative description presented for absorption of radiation in the Schumann-Runge bands and Herzberg continuum of O₂ was shown to be consistent with both laboratory and in situ atmospheric measurements. Rates for photolysis of N₂O, CFCl₃, and CF₂Cl₂ exhibit a demonstrable sensitivity to the magnitude and spectral dependence of the attenuation of solar ultraviolet by O₂. A high-resolution transmission model was used, in combination with height and latitudinal distributions of N₂O, CFCl₃, and CF₂Cl₂, to evaluate lifetimes and to infer rates for production of these gases in 1980. Lifetimes calculated here are significantly shorter (123, 44, and 116 years for N₂O, CFCl₃, and CF₂Cl₂, respectively) and source rates correspondingly higher than values obtained in previous studies. Global emissions of N₂O, CFCl₃, and CF₂Cl₂ were estimated at 1.52×10^{10} kg N yr⁻¹, 2.47×10^8 kg Cl yr⁻¹, and 2.41×10^8 kg Cl yr⁻¹, respectively. It appears that the contemporary source of N₂O is larger than the preindustrial value by about 31%. Emission rates estimated for CFCl₃ and CF₂Cl₂ in 1980 are about 21% and 5% larger, respectively, than values estimated by industry.

The budget of stratospheric odd oxygen was reexamined using an updated treatment of data from the ATMOS experiment. The photochemical model was shown to provide good agreement with the suite of photochemically reactive species observed in this experiment both for 30°N and 47°S during northern sum-

mer. It was necessary, in order to account for relative abundances observed for ClNO₃ and HCl, to invoke an additional source of HCl, attributed here to reaction of ClO and OH, equation (8). Careful analysis of rates for production and loss of odd oxygen confirmed the need for an additional source above about 40 km. This is especially important for the simulation at 30°N. The pattern of the missing source, specifically its variation with altitude and the apparent interhemispheric asymmetry, is consistent with production by photolysis of vibrationally excited O₂ as discussed by *Slanger et al.* [1988] and *Toumi et al.* [1991]. More generally it was shown to be compatible with a rate for production proportional to the product of the ozone mixing ratio and the frequency for photolysis of O₃ below 300 nm.

APPENDIX: OPACITY DISTRIBUTION FUNCTIONS

The computational expense associated with a line-by-line treatment of S-R band absorption is generally prohibitive for practical use in photochemical models. As a consequence, approximate methods have been devised to calculate O₂ photodissociation rates and the transmission of solar radiation in the wavelength range 175 to 200 nm [see *Simon and Brasseur*, 1983, and references therein]. The Harvard photochemical model [*Logan et al.*, 1978] utilizes opacity distribution functions (ODFs) to perform spectral integrations in wavelength intervals defined by successive S-R band heads [*Fang et al.*, 1974]. The contribution to the photodissociation frequency from a spectral interval, $\Delta\lambda_i$, is given by

$$J_{O_2}(z) = \int_{\Delta\lambda_i} I(\lambda) T(O_3, \lambda) \sigma(\lambda) e^{-\sigma(\lambda)N(z)} d\lambda \quad (A1)$$

where λ defines wavelength, $I(\lambda)$ the solar irradiance, $\sigma(\lambda)$ the S-R cross section, and $N(z)$ the slant-column abundance of O₂ at altitude z . Absorption by O₃ is taken into account using a transmission factor, $T(O_3, \lambda)$. Equation (A1) neglects complications due to variations in temperature over the extent of the absorbing column.

We propose to replace $I(\lambda)$ by an appropriate mean quantity, \bar{I} , defined with respect to the interval $\Delta\lambda_i$. A mean transmission factor for ozone can be similarly defined. Employing a statistical analysis of the distribution of $\sigma(\lambda)$ within the interval $\Delta\lambda_i$, we evaluate a probability density function $f(\sigma)$, such that $f(\sigma')d\sigma'$ is the probability that σ lies between σ' and $\sigma'+d\sigma'$ within the interval $\Delta\lambda_i$. Equation (A1) can be expressed then in the form

$$J_{O_2}(z) = \bar{I} \Delta\lambda_i T(O_3) \int_{\sigma_{\min}}^{\sigma_{\max}} \sigma' e^{-\sigma'N(z)} f(\sigma') d\sigma' \quad (A2)$$

This can be simplified further with a change of variable from σ to $g(\sigma)$, the opacity distribution function, given by

$$g(\sigma') = \int_0^{\sigma'} f(\sigma) d\sigma \quad (A3)$$

The ODF represents a cumulative probability function; $g(\sigma')$ is the fraction of the spectral interval occupied by

cross sections less than σ' . From equation (A3) we obtain

$$dg = f(\sigma') d\sigma' \quad (A4)$$

and equation (A2) may be rewritten in the form:

$$J_{O_2}(z) = \bar{I} \Delta\lambda_i T(O_3) \int_0^1 \sigma(g) e^{-\sigma(g)N(z)} dg \quad (A5)$$

Equation (A5) involves a reordering of quadrature points into a sequence of monotonically increasing values of σ . The economy of this approach is illustrated in Figures A1 and A2, where values of σ are shown as functions of λ and g , respectively, for the 7-0 S-R band at a temperature of 250 K. The number of quadrature points required to evaluate the photodissociation rate for the 7-0 band is reduced from about 1000 using the line-by-line approach to only six in the case of the ODF method of integration.

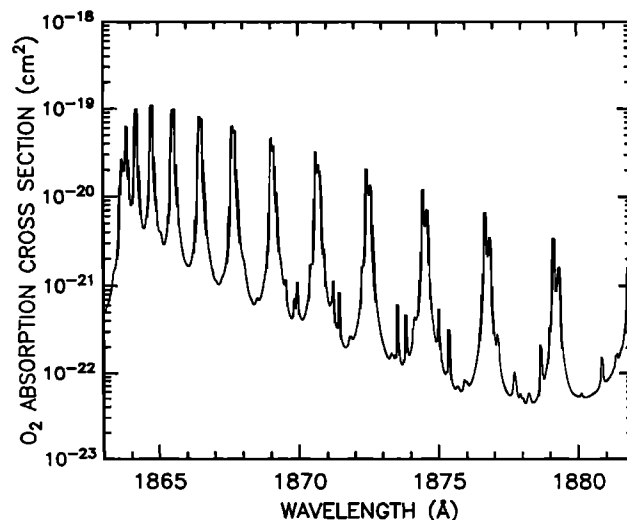


Fig. A1. Absorption cross section for O₂ calculated by the line-by-line model for a temperature of 250 K. The spectral interval (1863 to 1882 Å) spans the 7-0 Schumann-Runge band.

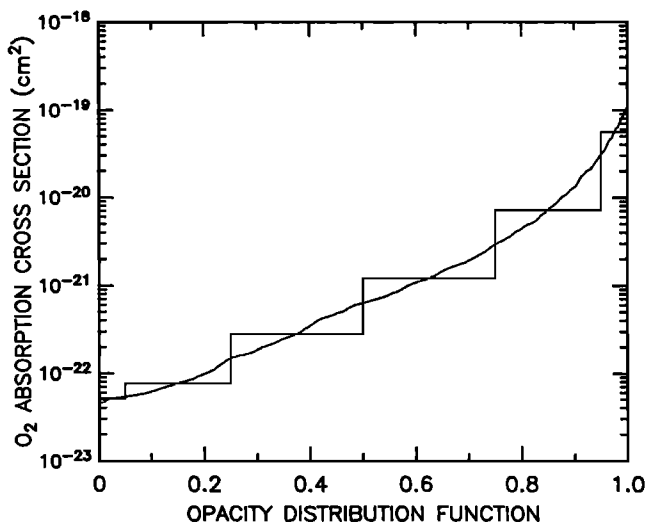


Fig. A2. The opacity distribution function calculated for the absorption cross section shown in Fig. A1. The histogram indicates the quadrature used to integrate $\sigma(g)$ in equation (A5).

TABLE A1. Opacity Distribution Functions

Interval, Å	T, K	Weight					
		0.05	0.20	0.25	0.25	0.20	0.05
1775 to 1783	205	1.03(-21)	1.75(-21)	4.59(-21)	1.71(-20)	1.01(-19)	1.10(-18)
1783 to 1793	210	7.68(-22)	1.24(-21)	2.67(-21)	1.08(-20)	8.36(-20)	7.70(-19)
1793 to 1804	205	1.13(-21)	2.02(-21)	4.66(-21)	1.65(-20)	9.30(-20)	5.02(-19)
1804 to 1816	205	5.56(-22)	1.58(-21)	3.72(-21)	1.38(-20)	7.22(-20)	3.44(-19)
1816 to 1831	235	2.97(-22)	5.83(-22)	2.05(-21)	8.19(-21)	4.80(-20)	2.66(-19)
1831 to 1846	220	1.35(-22)	2.99(-22)	7.33(-22)	3.07(-21)	1.69(-20)	1.66(-19)
1846 to 1863	225	1.08(-22)	2.09(-22)	5.88(-22)	2.59(-21)	1.58(-20)	1.03(-19)
1863 to 1882	235	4.49(-23)	6.68(-23)	2.38(-22)	1.13(-21)	6.99(-21)	5.55(-20)
1882 to 1902	250	1.91(-23)	3.44(-23)	1.17(-22)	4.74(-22)	2.65(-21)	2.53(-20)
1902 to 1925	265	1.12(-23)	2.45(-23)	7.19(-23)	3.04(-22)	1.75(-21)	1.11(-20)
1925 to 1947	250	9.60(-24)	1.26(-23)	2.55(-23)	1.05(-22)	5.19(-22)	2.82(-21)
1947 to 1972	235	6.82(-24)	7.50(-24)	1.03(-23)	2.48(-23)	1.52(-22)	1.25(-21)
1972 to 1985	230	6.98(-24)	7.49(-24)	9.31(-24)	1.65(-23)	7.87(-23)	4.63(-22)
1985 to 2000	225	6.74(-24)	6.77(-24)	6.93(-24)	7.36(-24)	1.04(-23)	5.18(-23)
2000 to 2025	225	6.84(-24)	6.85(-24)	6.88(-24)	7.11(-24)	8.41(-24)	2.87(-23)

Units for σ_j are in centimeters squared. The values in parenthesis refer to powers of ten.

The six subintervals represented by the histogram in Figure A2 show the integration quadrature employed in the Harvard photochemical model. The values of $\sigma(g)$ shown in the histogram are determined by the median values within each subinterval. We tested the accuracy of this choice of quadrature and found the approach to be robust; results using a 300-point ODF quadrature differed from the six point standard by no more than 1%.

There are two sources of error in applying ODFs to study absorption of ultraviolet radiation by O₂; they relate to the use of mean solar irradiances and the temperature dependence of S-R band cross sections. The first is minor provided that the solar irradiance and S-R band cross sections are uncorrelated within a given spectral interval. The second can be more serious if care is not taken to select the appropriate temperature for evaluation of S-R band cross sections. The objective is to minimize errors in transmission of ultraviolet radiation as they may affect rates for photolysis. The total rate for photolysis depends on a sum of contributions from indi-

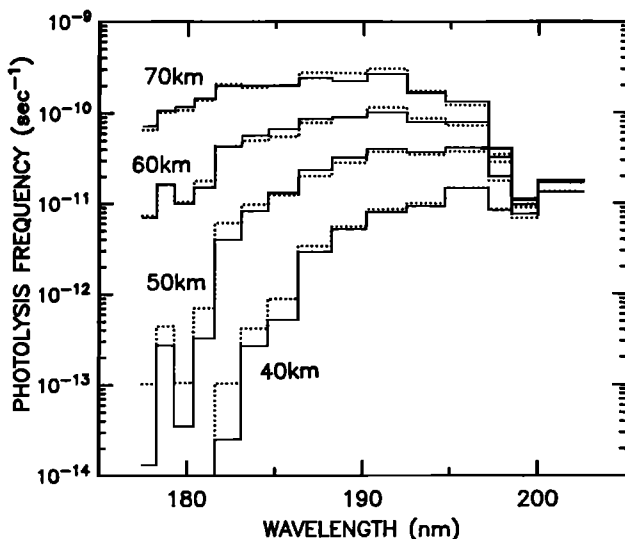


Fig. A3. Calculated photolysis frequencies for O₂ integrated over the spectral intervals given in Table A1, using the line-by-line model (solid lines) and the ODF formulation (dotted lines), for the atmospheric structure specified in the U.S. Standard Atmosphere (1976) and a solar zenith angle of 30°. Results are shown for altitudes of 70, 60, 50 and 40 km.

vidual spectral intervals. The partial photolysis rate of O₂ for a spectral interval $\Delta\lambda_i$ is given by equation (A5). For the case where the solar irradiance is independent of wavelength, it is easily shown that the contribution to the photodissociation rate is largest when the optical depth, σN , is equal to 1. Therefore for each spectral interval, the temperature chosen to define the ODF corresponds to the altitude at which $\sigma(g)N = 1$, for $g = 0.5$, using the U.S. Standard Atmosphere (1976) and a solar zenith angle of 30°. Table A1 gives values for the ODFs calculated in this manner. The appropriate weighting factors, defined by the width of individual subintervals (compare Figure A2), are given at the top of each column.

Using the results in Table A1, the spectrally integrated rate for photodissociation of O₂ in the S-R bands at altitude z is given by

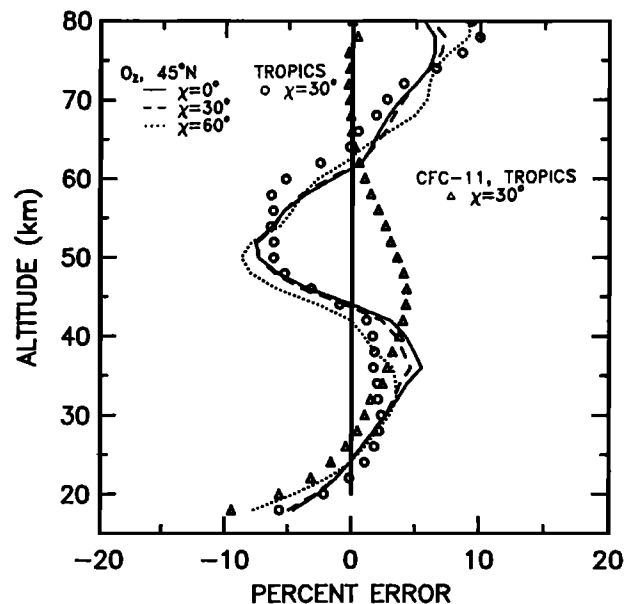


Fig. A4. Percent difference between photolysis frequencies of O₂ found using the ODF method as compared with line-by-line results. The solid, dashed, and dotted curves refer to differences for the photolysis frequencies of O₂ using the atmospheric structure of the U.S. Standard Atmosphere (1976), for solar zenith angles (χ) of 0°, 30° and 60°, respectively. The circles and triangles denote differences in the photolysis frequencies of O₂ and CFC₁₁, respectively, for the tropical atmosphere [Anderson *et al.*, 1986] and $\chi = 30^\circ$.

$$J_{O_2}(z) = \sum_{i=1}^{15} \bar{I}_i \Delta\lambda_i T(O_3)_i \sum_{j=1}^6 \sigma_{i,j} e^{-\sigma_{i,j} N(z)} W_j \quad (A6)$$

where i refers to the individual wavelength interval, and W_j is the weighting factor for the ODF subinterval j . The mean solar irradiance at level z for a specific interval, i , is given by

$$\bar{I}_i(z) = \bar{I}_i T(O_3)_i \sum_{j=1}^6 e^{-\sigma_{i,j} N(z)} W_j \quad (A7)$$

and is used to compute photodissociation frequencies for minor constituents.

Figure A3 presents a comparison of rates for photolysis of O₂ calculated using the ODF approach with values obtained using the numerically exact line-by-line standard. Specifically, it illustrates the contribution of individual spectral intervals to the rate for photolysis of O₂ at altitudes of 40, 50, 60, and 70 km. We allowed for absorption by O₃ using cross sections from *DeMore et al.* [1990], with temperatures, densities, and concentrations of ozone taken from the U.S. Standard Atmosphere (1976). Solar irradiances were specified on the basis of SUSIM measurements [VanHoosier et al., 1988]. We employed the full resolution of the SUSIM data (0.15-nm band pass) for line-by-line calculations, while mean values of irradiance were evaluated for individual spectral intervals for the ODF approach. Photolysis rates obtained using the ODF formulation agree with the line-by-line calculations for individual spectral intervals to within 15%, except for isolated cases where the contribution from a particular spectral interval to the total photodissociation rate is too small to be important.

It is apparent from Figure A3 that differences between the line-by-line and ODF results are generally small for intervals where photolysis rates are largest. Errors in total photodissociation rates, presented in Figure A4 for zenith angles of 0°, 30° and 60°, are less than 10% throughout the altitude range 20 to 80 km. Nearly all of the error associated with the use of the ODFs in Table A1 may be attributed to the choice of a single temperature to characterize the S-R cross section in individual spectral intervals. For example, the wavelength interval 190.2 to 192.5 nm is important in determining J_{O_2} over the entire altitude range from 40 to 80 km (Figure A3); the choice of temperature for the cross section in this interval (265 K, ~ 54 km) represents the best compromise in minimizing systematic errors throughout the altitude range 40 to 80 km. The overall level of agreement between the line-by-line and ODF results is remarkable considering that the ODFs employ only 90 values in toto for the cross section compared with almost 14,000 for the line-by-line calculation. The savings in execution time, based on our benchmark tests, is at least a factor of 100.

Acknowledgments. We thank G. P. Anderson and A. Hall for useful discussions and for providing data from their balloon measurements. We appreciate helpful discussions with S. C. Wofsy, C. E. Kolb, and T. G. Slanger. We are grateful also to J. Lean for making available results from the SUSIM experiment. This work was supported by NSF grant ATM-89-21119 and NASA grant NAGW-1230 to Harvard University. K. Minschwaner was supported by a fellowship from the Alexander Host Foundation.

REFERENCES

- Ackerman, M., F. Biaume, and G. Kockarts, Absorption cross sections of the Schumann-Runge bands of molecular oxygen, *Planet Space Sci.*, **18**, 1638-1651, 1970.
- Allen, M., and M. L. Delitsky, Stratospheric NO, NO₂, and N₂O₅: A comparison of model results with Spacelab 3 Atmospheric Trace Molecule (ATMOS) measurements, *J. Geophys. Res.*, **95**, 14077-14082, 1990.
- Allen, M., and M. L. Delitsky, A test of odd-oxygen photochemistry using Spacelab 3 Atmospheric Trace Molecule Spectroscopy observations, *J. Geophys. Res.*, **96**, 12883-12891, 1991.
- Allison, A. C., A. Dalgarno, and N. W. Pasachoff, Absorption by vibrationally excited molecular oxygen in the Schumann-Runge continuum, *Planet. Space Sci.*, **19**, 1463-1473, 1971.
- Anderson, G. P., and L. A. Hall, Attenuation of solar irradiance in the stratosphere: Spectrometer measurements between 191 and 207 nm, *J. Geophys. Res.*, **88**, 6801-6806, 1983.
- Anderson, G. P., and L. A. Hall, Stratospheric determination of O₂ cross sections and photodissociation rate coefficients: 191-215 nm, *J. Geophys. Res.*, **91**, 14509-14514, 1986.
- Anderson, G. P., S. A. Clough, F. X. Kneizys, J. H. Chetwynd, and E. P. Shettle, AFGL atmospheric constituent profiles (0-120 km), *Rep. AFGL-TR-86-0110*, 43 pp., Air Force Geophys. Lab., Hanscom AFB, Mass., 1986.
- Brasseur, G., A. De Rudder, and C. Tricot, Stratospheric response to chemical perturbations, *J. Atmos. Chem.*, **3**, 261-288, 1985.
- Brix, P., and G. Herzberg, Fine structure of the Schumann-Runge bands near the convergence limit and the dissociation energy of the oxygen molecule, *Can. J. Phys.*, **32**, 110-135, 1954.
- Brune, W. H., E. M. Weinstock, and J. G. Anderson, Mid-latitude ClO below 22 km altitude: Measurements with a new aircraft-borne instrument, *Geophys. Res. Lett.*, **15**, 144-147, 1988.
- Burnett, C. R., K. R. Minschwaner, and E. B. Burnett, Vertical column measurements of atmospheric hydroxyl from 26°, 40°, and 65°N, *J. Geophys. Res.*, **93**, 5241-5253, 1988.
- Cadle, R. D., P. Crutzen, and D. Ehhalt, Heterogeneous chemical reactions in the stratosphere, *J. Geophys. Res.*, **80**, 3381-3385, 1975.
- Chance, K. V., D. G. Johnson, and W. A. Traub, Measurement of stratospheric HOCl: Concentration profiles, including diurnal variation, *J. Geophys. Res.*, **94**, 11059-11069, 1989.
- Chandra, S., C. H. Jackman, A. R. Douglass, E. L. Fleming, and D. B. Considine, Chlorine catalyzed destruction of ozone: Implications for ozone variability in the upper stratosphere, *Geophys. Res. Lett.*, **20**, 351-354, 1993.
- Chemical Manufacturers Association, World production and release of chlorofluorocarbons 11 and 12 through 1981, Report, Fluorocarbon Program Panel, Washington, D. C., 1982.
- Cheung, A. S.-C., K. Yoshino, W. H. Parkinson, and D. E. Freeman, Herzberg continuum cross section of oxygen in the wavelength region 193.5-204 nm: New laboratory measurements and stratospheric implications, *Geophys. Res. Lett.*, **11**, 580-582, 1984.
- Cheung, A. S.-C., K. Yoshino, W. H. Parkinson, and D. E. Freeman, Molecular spectroscopic constants of O₂(B₃Σ_g⁻): The upper state of the Schumann-Runge bands, *J. Mol. Spectrosc.*, **119**, 1-10, 1986a.
- Cheung, A. S.-C., K. Yoshino, W. H. Parkinson, S. L. Guberman, and D. E. Freeman, Absorption cross section measurements of oxygen in the wavelength region 195-241 nm of the Herzberg continuum, *Planet. Space Sci.*, **34**, 1007-1016, 1986b.
- Cheung, A. S.-C., K. Yoshino, D. E. Freeman, R. S. Friedman, A. Dalgarno, and W. H. Parkinson, The Schumann-Runge bands of ¹⁶O¹⁸O in the wavelength region 175-205 nm and the spectroscopic constants of isotopic oxygen molecules, *J. Mol. Spectrosc.*, **134**, 362-389, 1989.
- Cheung, A. S.-C., K. Yoshino, J. R. Esmond, S. S.-L. Chiu, D. E. Freeman, and W. H. Parkinson, Predissociation line widths of the (1,0) - (12,0) Schumann-Runge absorption bands of O₂ in the wavelength region 179-202 nm, *J. Chem. Phys.*, **92**, 842-849, 1990.
- Chiu, S. S.-L., A. S.-C. Cheung, K. Yoshino, J. R. Esmond, D. E. Freeman, and W. H. Parkinson, Predissociation line widths of the (3,0) - (11,0) Schumann-Runge absorption bands of ¹⁸O₂ and ¹⁶O¹⁸O in the wavelength region 180-196 nm, *J. Chem. Phys.*, **93**, 5539-5543, 1990.
- Clancy, R. T., D. W. Rusch, and R. J. Thomas, Model ozone photochemistry on the basis of Solar Mesosphere Explorer observations, *J. Geophys. Res.*, **92**, 3067-3080, 1987.
- Crutzen, P. J., and U. Schmailzl, Chemical budgets of the stratosphere, *Planet. Space Sci.*, **31**, 1009-1032, 1983.
- Cunnold, D. M., R. G. Prinn, R. A. Rasmussen, P. G. Simmonds, F. N. Alyea, C. A. Cardelino, A. J. Crawford, P. J. Fraser, and R. D. Rosen, The Atmospheric Lifetime Experiment 3. Lifetime methodology and

- application to three years of CFC₁₃ data, *J. Geophys. Res.*, **88**, 8379–8400, 1983a.
- Cunnold, D. M., R. G. Prinn, R. A. Rasmussen, P. G. Simmonds, F. N. Aleya, C. A. Cardelino, and A. J. Crawford, The Atmospheric Lifetime Experiment, 4, Results for CF₂Cl₂ based on three years data, *J. Geophys. Res.*, **88**, 8401–8414, 1983b.
- DeMore, W. B., S. P. Sander, D. M. Golden, M. J. Molina, R. F. Hampson, M. J. Kurylo, C. J. Howard, and A. R. Ravishankara, Chemical kinetics and photochemical data for use in stratospheric modeling, Evaluation No. 9, *JPL Pub. 90-1*, Jet Propul. Lab., Pasadena, Calif., 1990.
- Fabian, P., R. Borchers, G. Flentje, W. A. Matthews, W. Seiler, H. Giehl, K. Bunse, F. Müller, U. Schmidt, A. Volz, A. Khedim, and F. J. Johnen, The vertical distribution of stable trace gases at mid-latitudes, *J. Geophys. Res.*, **86**, 5179–5184, 1981.
- Fang, T. M., S. C. Wofsy, and A. Dalgarno, Opacity distribution functions and absorption in the Schumann-Runge bands of molecular oxygen, *Planet. Space Sci.*, **22**, 413–425, 1974.
- Farmer, C. B., O. F. Raper, B. D. Robbins, R. A. Toth, and C. Muller, Simultaneous spectroscopic measurements of stratospheric species: O₃, CH₄, CO, CO₂, N₂O, H₂O, HCl, and HF at northern and southern mid-latitudes, *J. Geophys. Res.*, **85**, 1621–1632, 1980.
- Farmer, C. B., O. F. Raper, F. G. O'Callaghan, Final report on the first flight of the ATMOS instrument during the Spacelab 3 mission, April 29 through May 6, 1985, *JPL Pub. 87-32*, Jet Propul. Lab., Pasadena, Calif., 1987.
- Frederick, J. E., and R. D. Hudson, Predissociation line widths and oscillator strengths for the 2-0 to 13-0 Schumann-Runge bands of O₂, *J. Mol. Spectrosc.*, **74**, 247–256, 1979.
- Frederick, J. E., and R. D. Hudson, Dissociation of molecular oxygen in the Schumann-Runge bands, *J. Atmos. Sci.*, **37**, 1099–1106, 1980.
- Frederick, J. E., and J. E. Mentall, Solar irradiance in the stratosphere: Implications for the Herzberg continuum absorption of O₂, *Geophys. Res. Lett.*, **9**, 461–464, 1982.
- Froidevaux, L., and Y. L. Yung, Radiation and chemistry in the stratosphere: Sensitivity to O₂ absorption cross sections in the Herzberg continuum, *Geophys. Res. Lett.*, **9**, 854–857, 1982.
- Froidevaux, L., M. Allen, and Y. L. Yung, A critical analysis of ClO and O₃ in the mid-latitude stratosphere, *J. Geophys. Res.*, **90**, 12999–13029, 1985.
- Froidevaux, L., M. Allen, S. Berman, and A. Daughton, The mean ozone profile and its temperature sensitivity in the upper stratosphere and lower mesosphere: An analysis of LIMN observations, *J. Geophys. Res.*, **94**, 6389–6417, 1989.
- Gallagher, C. C., C. A. Forsberg, and R. V. Pieri, Stratospheric N₂O, CF₂Cl₂, and CFC₁₃ composition studies utilizing in situ cryogenic, whole air sampling methods, *J. Geophys. Res.*, **88**, 3798–3808, 1983.
- Goldan, P. D., W. C. Kuster, D. L. Albritton, and A. L. Schmeltekopf, Stratospheric CFC₁₃, CF₂Cl₂, and N₂O height profile measurements at several latitudes, *J. Geophys. Res.*, **85**, 413–423, 1980.
- Goldan, P. D., W. C. Kuster, A. L. Schmeltekopf, F. C. Fehsenfeld, and D. L. Albritton, Correction of atmospheric N₂O mixing ratio data, *J. Geophys. Res.*, **86**, 5385–5386, 1981.
- Gunson, M. R., C. B. Farmer, R. H. Norton, R. Zander, C. P. Rinsland, J. H. Shaw, and B.-G. Gao, Measurements of CH₄, N₂O, CO, H₂O, and O₃ in the middle atmosphere by the ATMOS experiment on Spacelab 3, *J. Geophys. Res.*, **95**, 13867–13882, 1990.
- Guthrie, P. D., C. H. Jackman, T. L. Kucsera, and J. E. Rosenfield, On the sensitivity of a residual circulation model to differences in input temperature data, *J. Geophys. Res.*, **95**, 873–882, 1990.
- Hasson, V., and R. W. Nicholls, Absolute spectral absorption measurements on molecular oxygen from 2460 to 1920 Å: continuum measurements 2430–1920 Å, *J. Phys. B. A. Mol. Phys.*, **4**, 1789–1797, 1971.
- Heidt, L. E., R. Lueb, W. Pollock, and D. H. Ehhalt, Stratospheric profiles of CCl₃F and CCl₂F₂, *Geophys. Res. Lett.*, **2**, 445–447, 1975.
- Herman, J. R., and J. E. Mentall, O₂ absorption cross sections (187–225 nm) from stratospheric solar flux measurements, *J. Geophys. Res.*, **87**, 8967–8975, 1982.
- Hudson, R. D., and V. L. Carter, Absorption of oxygen at elevated temperatures (300 to 900 K) in the Schumann-Runge system, *J. Opt. Soc. Am.*, **58**, 1621–1629, 1968.
- Hudson, R. D., and S. H. Mahle, Photodissociation rates of molecular oxygen in the mesosphere and lower thermosphere, *J. Geophys. Res.*, **77**, 2902–2914, 1972.
- Jackman, C. H., and P. D. Guthrie, Sensitivity of N₂O, CFC₁₃, and CF₂Cl₂ two-dimensional distributions to O₂ absorption cross sections, *J. Geophys. Res.*, **90**, 3919–3923, 1985.
- Jackman, C. H., R. S. Stolarski, and J. A. Kaye, Two-dimensional monthly average ozone balance from Limb Infrared Monitor of the Stratosphere and Stratospheric and Mesospheric Sounder data, *J. Geophys. Res.*, **91**, 1103–1116, 1986.
- Jenouvrier, A., B. Coquart, and M. F. Merienne-Lafore, New measurements of the absorption cross sections in the Herzberg continuum of molecular oxygen in the region between 205 and 240 nm, *Planet. Space Sci.*, **34**, 253–254, 1986a.
- Jenouvrier, A., B. Coquart, and M. F. Merienne, Long path length measurements of oxygen absorption cross sections in the wavelength region 205–240 nm, *J. Quant. Spectrosc. Radiat. Transfer*, **36**, 349–354, 1986b.
- Johnston, H. S., O. Serang, and J. Podolske, Instantaneous global nitrous oxide photochemical rates, *J. Geophys. Res.*, **84**, 5077–5082, 1979.
- Johnston, H. S., M. Paige, and F. Yao, Oxygen absorption cross sections in the Herzberg continuum and between 206 and 327 K, *J. Geophys. Res.*, **89**, 11661–11665, 1984.
- Jones, R. L., and J. A. Pyle, Observations of CH₄ and N₂O by the NIMBUS 7 SAMS: A comparison with in situ data and two-dimensional numerical model calculations, *J. Geophys. Res.*, **89**, 5263–5279, 1984.
- Kao, C.-Y. J., X. Tie, E. Mroz, D. Cunnold, and F. Aleya, Simulation of the global CFC 11 using the Los Alamos chemical tracer model, *J. Geophys. Res.*, **97**, 15827–15838, 1992.
- Kingawa, T., S. Tetsuya, and T. Arikawa, Formations of O(³P) photofragments from the Hartley band photodissociation of ozone at 226 nm, *J. Chem. Phys.*, **93**, 3289–3294, 1990.
- Khalil, M. A. K., and R. A. Rasmussen, Nitrous oxide: Trends and global mass balance over the last 3000 years, *Ann. Glaciol.*, **10**, 73–79, 1988.
- Ko, M. K. W., and N. D. Sze, A 2-D model calculation of atmospheric lifetimes for N₂O, CFC-11 and CFC-12, *Nature*, **297**, 317–319, 1982.
- Ko, M. K. W., N. D. Sze, and D. K. Weisenstein, Use of satellite data to constrain the model-calculated atmospheric lifetime for N₂O: Implications for other trace gases, *J. Geophys. Res.*, **96**, 7547–7552, 1991.
- Kockarts, G., Penetration of solar radiation in the Schumann-Runge bands of molecular oxygen, in *Mesospheric Models and Related Experiments*, edited by G. Fiocco, pp. 160–176, D. Reidel, Norwell, Mass., 1971.
- Lewis, B. R., L. Berzins, and J. H. Carver, Decomposition of the photoabsorption continuum underlying the Schumann-Runge bands of ¹⁶O₂, I, Role of the B³Σ_u⁻ state: a new dissociation limit, *J. Quant. Spectrosc. Radiat. Transfer*, **33**, 627–643, 1985a.
- Lewis, B. R., L. Berzins, and J. H. Carver, Decomposition of the photoabsorption continuum underlying the Schumann-Runge bands of ¹⁶O₂, II, Role of the I³Π_u state and collision-induced absorption, *J. Quant. Spectrosc. Radiat. Transfer*, **34**, 405–415, 1985b.
- Lewis, B. R., L. Berzins, and J. H. Carver, Oscillator strengths for the Schumann-Runge bands of O₂, *J. Quant. Spectrosc. Radiat. Transfer*, **36**, 209–232, 1986a.
- Lewis, B. R., L. Berzins, J. H. Carver, and S. T. Gibson, Rotational variation of predissociation linewidth in the Schumann-Runge bands of ¹⁶O₂, *J. Quant. Spectrosc. Radiat. Transfer*, **36**, 187–207, 1986b.
- Logan, J. A., M. J. Prather, S. C. Wofsy, and M. B. McElroy, Atmospheric chemistry: Response to human influence, *Philos. Trans. R. Soc. London, Ser. A*, **290**, 187–234, 1978.
- McElroy, M. B., Chemical processes in the solar system: A kinetic perspective, in *M. T. P. International Review of Science*, Ser. 2, vol. 9, edited by D. Herschbach, Butterworths, London, 1976.
- McElroy, M. B., and R. J. Salawitch, Changing composition of the global stratosphere, *Science*, **243**, 763–770, 1989a.
- McElroy, M. B., and R. J. Salawitch, Stratospheric ozone: Impact of human activity, *Planet. Space Sci.*, **37**, 1653–1672, 1989b.
- McElroy, M. B., R. J. Salawitch, and K. Minschwaner, The changing stratosphere, *Planet. Space Sci.*, **40**, 373–401, 1992.
- Minschwaner, K., G. P. Anderson, L. A. Hall, and K. Yoshino, Polynomial coefficients for calculating O₂ Schumann-Runge cross sections at 0.5 cm⁻¹ resolution, *J. Geophys. Res.*, **97**, 10103–10108, 1992.
- Murtagh, D. P., The O₂ Schumann-Runge system: New calculations of photodissociation cross sections, *Planet. Space Sci.*, **36**, 819–828, 1988.
- Natarajan, M., and L. B. Callis, Examination of stratospheric ozone photochemistry in light of recent data, *Geophys. Res. Lett.*, **16**, 473–476, 1989.
- Natarajan, M., and L. B. Callis, Stratospheric photochemical studies with Atmospheric Trace Molecule Spectroscopy (ATMOS) measurements, *J. Geophys. Res.*, **96**, 9361–9370, 1991.
- Natarajan, M., L. B. Callis, R. E. Boughner, J. M. Russel, and J. D. Lam-

- beth, Stratospheric photochemical studies using Nimbus 7 data, 1, Ozone photochemistry, *J. Geophys. Res.*, *91*, 1153–1166, 1986.
- Nicolet, M., and R. Kennes, Aeronomic problems of the molecular oxygen photodissociation, I, The O₂ Herzberg continuum, *Planet. Space Sci.*, *34*, 1043–1059, 1986.
- Nicolet, M., and R. Kennes, Aeronomic problems of the molecular oxygen photodissociation, III, Solar spectral irradiances in the region of the O₂ Herzberg continuum, Schumann-Runge bands and continuum, *Planet. Space Sci.*, *36*, 1059–1068, 1988.
- Nicolet, M., and R. Kennes, Aeronomic problems of molecular oxygen photodissociation, IV, Photodissociation frequency and transmittance in the spectral range of the Schumann-Runge bands, *Planet. Space Sci.*, *37*, 459–491, 1989.
- Nicolet, M., and W. Peetermans, Atmospheric absorption in the O₂ Schumann-Runge band spectral range and photodissociation rates in the stratosphere and mesosphere, *Planet. Space Sci.*, *28*, 85–103, 1980.
- Park, J. H., The equivalent mean absorption cross sections for the O₂ Schumann-Runge bands: Application to the H₂O and NO photodissociation rates, *J. Atmos. Sci.*, *31*, 1893–1897, 1974.
- Prather, M. J., M. B. McElroy, and S. C. Wofsy, Reductions in ozone at high concentrations of stratospheric halogens, *Nature*, *312*, 227–231, 1984.
- Raper, O. F., C. B. Farmer, R. Zander, and J. H. Park, Infrared spectroscopic measurements of halogenated sink and reservoir gases in the stratosphere with the ATMOS instrument, *J. Geophys. Res.*, *92*, 9851–9858, 1987.
- Rinsland, C. P., G. C. Toon, C. B. Farmer, R. H. Norton, and J. S. Namkung, Stratospheric N₂O₅ profiles at sunrise and sunset from further analysis of the ATMOS/Spacelab 3 solar spectra, *J. Geophys. Res.*, *94*, 18341–18349, 1989.
- Russell, J. M., III, C. B. Farmer, C. P. Rinsland, R. Zander, L. Froidevaux, G. C. Toon, B. Gao, J. Shaw, and M. Gunson, Measurements of odd nitrogen compounds in the stratosphere by the ATMOS experiment on Spacelab 3, *J. Geophys. Res.*, *93*, 1718–1736, 1988.
- Schmidt, U., and A. Khedim, In situ measurements of carbon dioxide in the winter Arctic vortex and at mid-latitudes: An indicator of the 'age' of stratospheric air, *Geophys. Res. Lett.*, *18*, 763–766, 1991.
- Shardanand, and A. D. Prasad Rao, Collision-induced absorption of O₂ in the Herzberg continuum, *J. Quant. Spectrosc. Radiat. Transfer*, *17*, 433–439, 1977.
- Simon, P. C., and G. Brasseur, Photodissociation effects of solar U.V. radiation, *Planet. Space Sci.*, *31*, 987–999, 1983.
- Slanger, T. G., L. E. Jusinski, G. Black, and G. E. Gadd, A new laboratory source of ozone and its potential atmospheric implications, *Science*, *241*, 945–950, 1988.
- Solomon, S., D. W. Rusch, R. J. Thomas, and R. S. Eckman, Comparison of mesospheric ozone abundances measured by the solar mesosphere explorer and model calculations, *Geophys. Res. Lett.*, *10*, 249–252, 1983.
- Stachnik, R. A., J. C. Hardy, J. A. Tarsala, J. W. Waters, and N. R. Erickson, Submillimeter heterodyne measurements of stratospheric ClO, HCl, and HO₂: First results, *Geophys. Res. Lett.*, *19*, 1931–1934, 1992.
- Toumi, R., An evaluation of autocatalytic ozone production from vibrationally excited oxygen in the middle atmosphere, *J. Atmos. Chem.*, *15*, 69–77, 1992.
- Toumi, R., B. J. Kerridge, and J. A. Pyle, Highly vibrationally excited oxygen as a potential source of ozone in the upper stratosphere and mesosphere, *Nature*, *351*, 217–219, 1991.
- Traub, W. A., D. G. Johnson, and K. V. Chance, Stratospheric hydroperoxyl measurements, *Science*, *247*, 446–449, 1990.
- VanHoosier, M. E., J.-D. F. Bartoe, G. E. Brueckner, and D. K. Prinz, Absolute solar spectral irradiance 120 nm–400 nm (results from the Solar Ultraviolet Spectral Irradiance Monitor–SUSIM–experiment on board Spacelab 2), *Astrophys. Lett. Commun.*, *27*, 163–168, 1988.
- Vedder, J. F., E. C. Y. Inn, B. J. Tyson, and C. A. Boitnott, Measurements of CF₂Cl₂, CFCl₃, and N₂O in the lower stratosphere between 2°S and 73°N latitude, *J. Geophys. Res.*, *86*, 7363–7368, 1981.
- Weinstock, E. M., M. J. Phillips, and J. G. Anderson, In situ observations of ClO in the stratosphere: A review of recent results, *J. Geophys. Res.*, *86*, 7273–7278, 1981.
- Weiss, R. F., The temporal and spatial distribution of tropospheric nitrous oxide, *J. Geophys. Res.*, *86*, 7185–7195, 1981.
- World Meteorological Organization (WMO), Global ozone research and monitoring project, *The stratosphere 1981; theory and measurements*, Rep. 11, Geneva, Switzerland, 1982.
- World Meteorological Organization (WMO), Global ozone research and monitoring project, *Atmospheric ozone 1985: Assessment of our understanding of the processes controlling its present distribution and change*, Rep. 16, Geneva, Switzerland, 1986.
- Yoshino, K., D. E. Freeman, J. R. Esmond, and W. H. Parkinson, High resolution absorption cross section measurements and band oscillator strengths of the (1,0)-(12,0) Schumann-Runge bands of O₂, *Planet. Space Sci.*, *31*, 339–353, 1983.
- Yoshino, K., D. E. Freeman, J. R. Esmond, and W. H. Parkinson, High resolution absorption cross sections and band oscillator strengths of the Schumann-Runge bands of oxygen at 79 K, *Planet. Space Sci.*, *35*, 1067–1075, 1987.
- Yoshino, K., A. S.-C. Cheung, J. R. Esmond, W. H. Parkinson, D. E. Freeman, and S. L. Guberman, Improved absorption cross sections of oxygen in the wavelength region 205–240 nm of the Herzberg continuum, *Planet. Space Sci.*, *36*, 1469–1475, 1988.
- Yoshino, K., D. E. Freeman, J. R. Esmond, R. S. Friedman, and W. H. Parkinson, High resolution absorption cross sections and band oscillator strengths of the Schumann-Runge absorption bands of isotopic oxygen, ¹⁶O¹⁸O, at 79 K, *Planet. Space Sci.*, *37*, 419–426, 1989.
- Yoshino, K., J. R. Esmond, A. S.-C. Cheung, D. E. Freeman, and W. H. Parkinson, Band oscillator strengths of the (2,1)-(12,1) Schumann-Runge Bands of O₂ from absolute absorption cross section measurements at room temperature, *J. Geophys. Res.*, *95*, 11743–11746, 1990.
- Yoshino, K., J. R. Esmond, A. S.-C. Cheung, D. E. Freeman, and W. H. Parkinson, High resolution absorption cross sections in the transmission window region of the Schumann-Runge bands and Herzberg continuum of O₂, *Planet. Space Sci.*, *40*, 185–192, 1992.
- Zander, R., M. R. Gunson, J. C. Foster, C. P. Rinsland, and J. Namkung, Stratospheric ClONO₂, HCl, HF concentration profiles derived from Atmospheric Trace Molecule Spectroscopy experiment Spacelab 3 observations: An update, *J. Geophys. Res.*, *95*, 20519–20525, 1990.

M.B. McElroy and R.J. Salawitch, Department of Earth and Planetary Sciences and Division of Applied Sciences, Pierce Hall, Harvard University, 29 Oxford Street, Cambridge, MA 02138.

K. Minschwaner, National Center for Atmospheric Research, P.O. Box 3000, Boulder, CO 80307.

(Received August 18, 1992;
revised December 31, 1992;
accepted January 20, 1993.)